*Robotica* (2023), **41**, pp. 3252–3274
doi:10.1017/S0263574723000747

CAMBRIDGE UNIVERSITY PRESS

RESEARCH ARTICLE

# Emergency ejection characteristics of space manipulator multi-body system

He Cai, Yanbo Wang, Songbo Deng and Tao Yang

Laboratory of Aerospace Servo Actuation and Transmission, Beijing Institute of Precision Mechatronics and Controls, Beijing, China
**Corresponding author:** Yanbo Wang; Email: www-2001@163.com

**Received:** 31 January 2023; **Revised:** 19 April 2023; **Accepted:** 3 May 2023; **First published online:** 14 August 2023

**Keywords:** ejection of space manipulator; equivalent ejection mass; ejection velocity; joint angular variation; ejection angular velocity

## Abstract

Space manipulators are typically installed on spacecraft using an emergency separation device (ESD). In the event of a malfunction, the ESD ejects the manipulator from the spacecraft. However, due to the relative rotation of the manipulator's joints during the ejection, the equivalent ejection mass varies depending on different attitudes. This paper focuses on studying manipulators equipped with separation slide rails and analyzes their ejection characteristics under different attitudes to determine the optimal manipulator attitude for ejection. Initially, the ejection dynamics model of the space manipulator is established using the Lagrangian method, based on the kinetic energy equation, kinematics equation, and the boundary condition between the manipulator and ESD. Afterward, the space dynamics model is transformed into the dynamic model of plane ejection state by recursion formula. From this model, the equivalent ejection mass and ejection velocity are obtained, and the joint angular variation during ejection is acquired by considering joint friction torque. Using the law of conservation of angular momentum, the ejection angular velocity is then calculated. Finally, this study selected a 7-DOF space manipulator as an example and adjusted the damping parameter $B$ of the joint for more precise calculations by choosing the attitude with a relatively larger joint angular variation. The modified model was then tested for its applicability to other attitudes. After determining the value of $B$, the correctness of the algorithm was validated by MATLAB calculation, ADAMS simulation, and real object ejection test.

## 1. Introduction

The space industry has entered a new phase marked by space resource exploitation and large-scale deep space detection. The global space industry will usher in the age of "flight transportation," which is to deploy aerospace vehicles as the carriers in the space transportation system. This allows mankind to enter and exit space freely, develop and utilize space resources, and find new space for survival and development. Meanwhile, the space manipulator is responsible for the modular operation of on-orbit devices and cargo maintenance transportation services [1, 2]. The emergency separation device (ESD) typically serves as the base to fix the manipulator on the spacecraft. However, when the manipulator or locking structure breaks down and cannot be returned to its initial position, the manipulator needs to be ejected for the safety of the spacecraft. In such instances, the ESD serves as the ejector of the space manipulator.

To avoid collision between the ejected manipulator and the spacecraft, a straight slide rail is deployed at the ESD to guide the manipulator's ejection along a straight line. Additionally, the optimal ejection attitude maximizes the ejection velocity of the manipulator. Unlike rigid body ejection, if the joints of the manipulator lose power and the ejection torque is larger than the static friction torque of the joints, they

may experience relative rotation. This can cause changes to the manipulator's configuration. Therefore, more research into the ejection characteristics for various attitudes is required. Jiang et al. [3, 4] studied the dynamics of centroid-biased on-orbit separation dynamics and proposed a method to restrain the angular velocity. In ref. [5–7], the jumping separation form of the robot is described from three aspects: one-legged hopping, water bouncing, and biped robot sliding jumping. Wang et al. [8] conducted the dynamic analysis of space ejection using separation slide rails deployed at random positions and solved the angular velocity problem caused by eccentricity. Zhang et al. [9] established a separation dynamic model of the space docking mechanism, identifying major factors influencing spacecraft separation attitude or velocity, including separation parameters, lock synchronization, and contact friction. Meanwhile, Zhang et al. [10] chose the cubic satellite as the subject in his study of on-orbit release movement and built an on-orbit release dynamic model to systematically analyze the nonlinear dynamic phenomenon. Last, Luo et al. [11] focused on the on-orbit separation of multi-rigid bodies, utilized the Lagrange multiplier to acquire the dynamics model, and achieved automatic separation using the ejection devices between every two rigid bodies.

The literature mentioned above investigated different separation scenarios, including the installation eccentricity, nonlinear dynamics, the use of linear slide rails to control angular velocity, and the ejection of every two rigid bodies in a multi-rigid body system. All of these studies were focused on spacecraft separation technologies. For regular combined rigid bodies, the relative positions and attitudes of each part are fixed during ejection, which means that the ejection mass equals the overall mass of the combined bodies. However, the joints of the manipulator have relative rotation during ejection, which can be converted into the equivalent mass according to the ejection dynamics model. The manipulator has different ejection characteristics depending on its attitude during ejection. Additionally, the ejection characteristics also change during the ejection process due to the change in the manipulator's attitude. This paper investigates the ejection characteristics of the manipulator in different attitudes, such as ejection equivalent mass, ejection velocity, joint angular variance, and ejection angular velocity. Furthermore, it probed into the impact of joint friction on ejection characteristics and subsequently adjusted the damping coefficient B in joint friction based on the results of the manipulator ejection test and applied the corrected coefficient to other attitudes.

## 2. Ejection dynamics modeling

### *2.1. Fundamental hypothesis*

During emergency ejection, the joints of a space manipulator may lose power and undergo relative rotation due to their limited back rotation torque. In this study, a multi-rigid body dynamics model of the space manipulator was established based on the dynamics of multi-rigid body systems. The ejection constraint of separation slide rails was also used as the boundary condition and the base ejection force as the generalized force. Then, the optimal ejection attitude of the manipulator was determined using the equivalent mass method [12]. Furthermore, the joint angular variance was computed by considering the joint friction characteristics. Following are the assumptions of this study.

1. The manipulator is regarded as a multi-rigid body without taking elastomer vibration in the arm rods and joints into account, and the manipulator's joints have no power during ejection.
2. The ejection dynamics model is built on the premise that the slide rail has sufficient support rigidity and no gaps. Furthermore, the slide rails are considered to have a smooth surface.
3. The spacecraft is taken as a large-mass rigid body equipped with an ESD. The mechanism has slide rails and is regarded as completely fixed and restricted. However, the impact on the rail during separation, as well as the mutual influence between the rail and the spacecraft, are not considered.
4. The analysis does not take into account the effects of gravity and other spatial perturbation factors.

https://doi.org/10.1017/S0263574723000747 Published online by Cambridge University Press

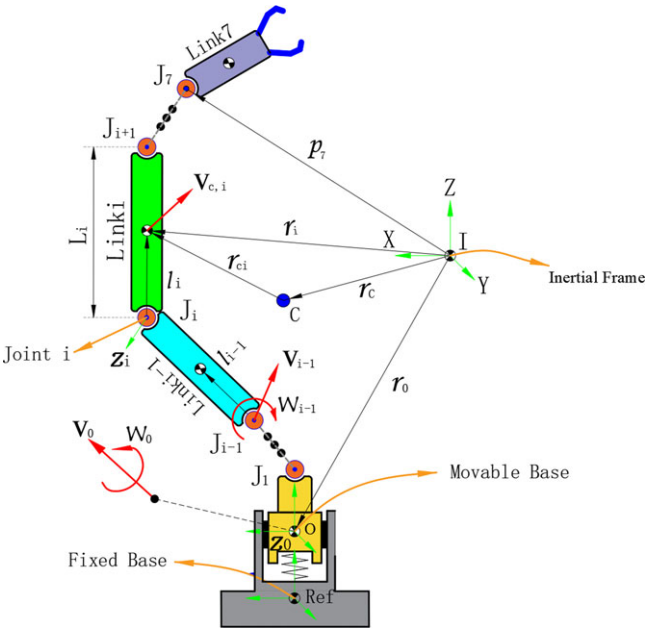


***Figure 1.*** *Schematic diagram of space ejection manipulator.*

### *2.2. Kinetic energy equation of space ejection manipulator*

The recursive formulas for the line velocity ${}^{i}\boldsymbol{v}_i$, angular velocity ${}^{i}\boldsymbol{\omega}_i$ and the center of mass line velocity ${}^{i}\boldsymbol{v}_{c,i}$ of the space manipulator arm $i$ are as follows:

$$\begin{aligned} {}^{i}\boldsymbol{v}_i &= {}^{i}_{i-1}\boldsymbol{R}\left({}^{i-1}\boldsymbol{v}_{i-1} + {}^{i-1}\boldsymbol{\omega}_{i-1} \times {}^{i-1}\boldsymbol{L}_{i-1}\right) \\ {}^{i}\boldsymbol{\omega}_i &= {}^{i}_{i-1}\boldsymbol{R}^{i-1}\boldsymbol{\omega}_{i-1} + \dot{\boldsymbol{\theta}}_i {}^{i}\boldsymbol{Z}_i \\ {}^{i}\boldsymbol{v}_{c,i} &= {}^{i}\boldsymbol{v}_i + {}^{i}\boldsymbol{\omega}_i \times {}^{i}\boldsymbol{l}_i \end{aligned} \tag{1}$$

where ${}^{i-1}\boldsymbol{L}_{i-1}$ is the vector from coordinates $i-1$ to coordinates $i$, $\dot{\boldsymbol{\theta}}_i$ is the angular velocity of the joint $i$, and ${}^{i}\boldsymbol{Z}_i$ is the axis direction of the joint $i$. ${}^{i}\boldsymbol{l}_i$ is the vector from the center of mass of the $i$th arm to the origin of its coordinate $i$.

Figure 1 presents the space 7-DOF manipulator and its dynamic parameters (all the following vectors are represented under the inertial frame I). The ESD comprises a fixed base and a movable base. The fixed base is mounted on the spacecraft, and the reference coordinate system (Ref) of the manipulator is located in the center of the fixed base, with the coordinate direction aligned with the direction of the inertial system. Meanwhile, the base coordinate system, located below the first joint of the manipulator, serves as the movable base. During ejection, the base coordinate system moves with a three-dimensional linear velocity vector $\boldsymbol{v}_0$ and angular velocity vector $\boldsymbol{\omega}_0$ relative to the Ref coordinate system [13, 14].

The total kinetic energy of the manipulator is the sum of kinetic energy generated by the linear velocity $T_v$ and angular velocity $T_\omega$ of all arms, and $\boldsymbol{I}_i$ is the inertia tensor of arm $i$:

$$T = T_\omega + T_v = \frac{1}{2}\sum_{i=0}^{7}\left((\boldsymbol{\omega}_i)^T \boldsymbol{I}_i \boldsymbol{\omega}_i + m_i(\boldsymbol{v}_i)^T \boldsymbol{v}_i\right) \tag{2}$$

The relationship between the total inertia matrix $\boldsymbol{H}$ and the kinetic energy of the system is

$$T = \frac{1}{2}\dot{\boldsymbol{\varphi}}^T \boldsymbol{H}(\varphi)\dot{\boldsymbol{\varphi}} \tag{3}$$

https://doi.org/10.1017/S0263574723000747 Published online by Cambridge University Press

where $\dot{\boldsymbol{\varphi}}$ is $\left[\boldsymbol{v}_0, \boldsymbol{\omega}_0, \dot{\boldsymbol{\theta}}\right]^T$. Both the linear velocity and angular velocity of the manipulator base are three-dimensional vectors. $m_i$ is the mass of the arm $i$, and M is the total mass of the manipulator. In Fig. 1, $\boldsymbol{r}_{0i}$ is the vector from the origin of the base coordinates 0 to the center of mass of the arm $i$. $\boldsymbol{r}_{0c}$ is the vector from the origin of the base coordinates 0 to the manipulator system centroid C:

$$\begin{aligned} \boldsymbol{r}_{0i} &= \boldsymbol{r}_i - \boldsymbol{r}_0 = \sum_{k=0}^{i-1} \boldsymbol{L}_k + \boldsymbol{l}_i \\ \boldsymbol{r}_{0c} &= \boldsymbol{r}_c - \boldsymbol{r}_0 = \frac{1}{M} \sum_{k=0}^{7} m_k \boldsymbol{r}_{0k} \end{aligned} \tag{4}$$

In the formula, $\boldsymbol{L}_i$ is the vector from the origin of the coordinates $i$ to the origin of the coordinates $i+1$, and $\boldsymbol{l}_i$ is the vector from the origin of the joint coordinates $i$ to the center of mass of the arm $i$.

Equation (1) is equivalent to Eqs. (5) and (6) in the inertial coordinates:

$$\begin{aligned} \boldsymbol{v}_i &= \boldsymbol{v}_0 + \omega_0 \times \boldsymbol{r}_{0i} + J_{vi} \cdot \dot{\boldsymbol{\theta}} \\ \boldsymbol{J}_{vi} \cdot \dot{\boldsymbol{\theta}} &= \sum_{k=1}^{i} \left[ \left( \boldsymbol{Z}_k \times \left( \boldsymbol{r}_i - \boldsymbol{p}_k \right) \right) \cdot \dot{\boldsymbol{\theta}}_k \right] \end{aligned} \tag{5}$$

where $\boldsymbol{J}_{vi}$ is the Jacobian matrix of the linear velocity at the center of mass of arm $i$:

$$\begin{aligned} \boldsymbol{\omega}_i &= \boldsymbol{\omega}_0 + \boldsymbol{J}_{\omega i} \cdot \dot{\boldsymbol{\theta}} \\ \boldsymbol{J}_{\omega i} \cdot \dot{\boldsymbol{\theta}} &= \sum_{k=1}^{i} \left( \boldsymbol{Z}_k \dot{\boldsymbol{\theta}}_k \right) \end{aligned} \tag{6}$$

where $\boldsymbol{J}_{\omega i}$ is the Jacobian matrix of the angular velocity at the center of mass of the arm $i$. By substituting Eqs. (4)–(6) into Eq. (2), $T_v$ and $T_\omega$ can be obtained and then can be combined with Eq. (3) to derive the total inertia matrix $\boldsymbol{H}$ of the space manipulator system:

$$\boldsymbol{H} = \begin{bmatrix} M\boldsymbol{E}_3 & M\left(\boldsymbol{r}_{oc}^*\right)^T & \sum_{i=1}^{7} m_i \boldsymbol{J}_{vi} \\ M r_{oc}^* & \sum_{i=0}^{7} \left[ \boldsymbol{I}_i + m_i \left(\boldsymbol{r}_{oi}^*\right)^T \boldsymbol{r}_{oi}^* \right] & \sum_{i=1}^{7} \left[ \boldsymbol{I}_i \boldsymbol{J}_{\omega i} - m_i \left(\boldsymbol{r}_{oi}^*\right)^T \boldsymbol{J}_{vi} \right] \\ \sum_{i=1}^{7} m_i (\boldsymbol{J}_{vi})^T & \sum_{i=1}^{7} \left[ (\boldsymbol{J}_{\omega i})^T \boldsymbol{I}_i - m_i (\boldsymbol{J}_{vi})^T \boldsymbol{r}_{oi}^* \right] & \sum_{i=1}^{7} \left[ (\boldsymbol{J}_{\omega i})^T \boldsymbol{I}_i \boldsymbol{J}_{\omega i} + m_i (\boldsymbol{J}_{vi})^T \boldsymbol{J}_{vi} \right] \end{bmatrix} \tag{7}$$

where $\boldsymbol{E}_3$ is a $3 \times 3$ identity matrix. If $\boldsymbol{r} = [a, b, c]$, then $\boldsymbol{r}^* = \begin{bmatrix} 0 & -c & b \\ c & 0 & -a \\ -b & a & 0 \end{bmatrix}$. For the 7-DOF manipulator, the matrix is $13 \times 13$ square matrix, including six movable base DOF and seven joints DOF.

### *2.3. Dynamic equation and equivalent mass of manipulator in space ejection state*

For the space manipulator, the absence of gravity implies that potential energy is not influenced by it. Moreover, the potential energy is considered to be zero, since the elastic vibration of the manipulator is not taken into account. According to the Lagrange equation of the second kind:

$$\begin{aligned} \boldsymbol{H}(\boldsymbol{\varphi})\ddot{\boldsymbol{\varphi}} + \boldsymbol{C}(\boldsymbol{\varphi}, \dot{\boldsymbol{\varphi}}) &= \boldsymbol{Q} \\ \boldsymbol{C}(\boldsymbol{\varphi}, \dot{\boldsymbol{\varphi}}) &= \dot{\boldsymbol{H}}(\boldsymbol{\varphi})\dot{\boldsymbol{\varphi}} - \frac{\partial}{\partial \varphi} \left[ \frac{1}{2} \dot{\boldsymbol{\varphi}}^T \boldsymbol{H}(\boldsymbol{\varphi}) \dot{\boldsymbol{\varphi}} \right] \end{aligned} \tag{8}$$

https://doi.org/10.1017/S0263574723000747 Published online by Cambridge University Press

where $\boldsymbol{C}(\boldsymbol{\varphi}, \dot{\boldsymbol{\varphi}}) = [\, \boldsymbol{c}_b \quad \boldsymbol{c}_r \,]^T$ is the nonlinear velocity-dependent term. The global inertia matrix of the dynamic equation is $\boldsymbol{H}$. Substitute the generalized force $\boldsymbol{Q}$ into Eq. (8), and let $\ddot{\boldsymbol{x}}_0 = [\, \dot{\boldsymbol{v}}_0 \quad \dot{\boldsymbol{\omega}}_0 \,]^T$ to obtain the ejection dynamic model of the space manipulator as follows:

$$\begin{bmatrix} \boldsymbol{H}_b & \boldsymbol{H}_{br} \\ \boldsymbol{H}_{br}^T & \boldsymbol{H}_r \end{bmatrix} \begin{bmatrix} \ddot{\boldsymbol{x}}_0 \\ \ddot{\boldsymbol{\theta}} \end{bmatrix} + \begin{bmatrix} \boldsymbol{c}_b \\ \boldsymbol{c}_r \end{bmatrix} = \begin{bmatrix} \boldsymbol{F}_b \\ \boldsymbol{\tau}_r \end{bmatrix} + \begin{bmatrix} \boldsymbol{J}_b^T \\ \boldsymbol{J}_r^T \end{bmatrix} \boldsymbol{F}_e \tag{9}$$

The force at the end $\boldsymbol{F}_e = 0$ when the space manipulator is ejected, and only the force $\boldsymbol{F}_b$ and the joint friction torque $\boldsymbol{\tau}_r = \boldsymbol{\tau}_f$ on the movable base is present:

$$\begin{aligned} \boldsymbol{H}_b \ddot{\boldsymbol{x}}_0 + \boldsymbol{H}_{br} \ddot{\boldsymbol{\theta}} + \boldsymbol{c}_b &= \boldsymbol{F}_b \\ \boldsymbol{H}_{br}^T \ddot{\boldsymbol{x}}_0 + \boldsymbol{H}_r \ddot{\boldsymbol{\theta}} + \boldsymbol{c}_r &= \boldsymbol{\tau}_f \end{aligned} \tag{10}$$

By eliminating the variable $\ddot{\boldsymbol{\theta}}$, the dynamic equation of the base coordinates can be obtained:

$$\tilde{\boldsymbol{H}}_b \ddot{\boldsymbol{x}}_0 + \tilde{\boldsymbol{J}}_b \boldsymbol{c}_b - \boldsymbol{c}_r = \tilde{\boldsymbol{J}}_b \boldsymbol{F}_b - \boldsymbol{\tau}_f \tag{11}$$

where $\tilde{\boldsymbol{H}}_b = \boldsymbol{H}_r \boldsymbol{H}_{br}^{-1} \boldsymbol{H}_b - \boldsymbol{H}_{br}^T, \tilde{\boldsymbol{J}}_b = \boldsymbol{H}_r \boldsymbol{H}_{br}^{-1}$. The nonlinear term change very small and can be ignored. Further, under the action of the slide rail and spring, the manipulator is ejected along the axis Z of the ESD without any rotation. The boundary conditions are as follows:

$$v_z \neq 0, \quad v_x = v_y = \omega_x = \omega_y = \omega_z = 0 \tag{12}$$

The expression of the global inertia matrix of the space manipulator ejection system that satisfies the condition is obtained by substituting the boundary condition into the global inertia matrix $\boldsymbol{H}$ as follows:

$$\begin{bmatrix} \boldsymbol{H}_b & \boldsymbol{H}_{br} \\ \boldsymbol{H}_{br}^T & \boldsymbol{H}_r \end{bmatrix} = \begin{bmatrix} M & \sum_{i=1}^{7} m_i \boldsymbol{e}_z^T \boldsymbol{J}_{vi} \\ \sum_{i=1}^{7} m_i (\boldsymbol{e}_z^T \boldsymbol{J}_{vi})^T & \sum_{i=1}^{7} [(\boldsymbol{J}_{\omega i})^T \boldsymbol{I}_i \boldsymbol{J}_{\omega i} + m_i (\boldsymbol{J}_{v_i})^T \boldsymbol{J}_{v_i}] \end{bmatrix} \tag{13}$$

In this case, $\dot{\boldsymbol{\varphi}}$ becomes $[v_z, \dot{\boldsymbol{\theta}}]^T$, $\boldsymbol{e}_z = [\, 0 \quad 0 \quad 1 \,]^T$. Here, we assume that friction torque $\boldsymbol{\tau}_f$ can be equivalently taken account as an inertial effect [15]. Let $\boldsymbol{\lambda} = diag[0, \lambda_1, \ldots, \lambda_7]$, Eq. (11) becomes

$$(\tilde{\boldsymbol{H}}_b + \boldsymbol{\lambda}) \ddot{\boldsymbol{x}}_0 = \tilde{\boldsymbol{J}}_b \boldsymbol{F}_b \tag{14}$$

Both the ejection force and the ejection direction of the movable base are in the Z direction. Let $\ddot{\boldsymbol{x}}_0 = \boldsymbol{e}_z \boldsymbol{a}_b, \boldsymbol{F}_b = \boldsymbol{e}_z F_b$, and substitute into Eq. (14), the equivalent mass of the manipulator is

$$m_b = \boldsymbol{e}_z^T \tilde{\boldsymbol{J}}_b^{-1} (\tilde{\boldsymbol{H}}_b + \boldsymbol{\lambda}) \boldsymbol{e}_z = \boldsymbol{e}_z^T \check{\boldsymbol{H}}_b \boldsymbol{e}_z \tag{15}$$

By substituting the corresponding terms of Eq. (13) into Eq. (14), the matrix $\check{\boldsymbol{H}}_b$ is obtained. $\boldsymbol{\lambda}$ can be obtained by combining Eqs. (11) and (14).

### *2.4. Equivalent mass of manipulator in plane ejection state*

The ejection test of the space manipulator is based on the air-floating platform [16, 17] and is supported by air-floating support as shown in Fig. 2. The ejection force $F_b$ is along the Z direction of Figs. 1 and 2. During the ejection in this state, the ejection force is coplanar with the axes of joints 1, 3, 5, and 7 and produces no additional torque. As a result, joints 1, 3, 5, and 7 are equivalent to fixed.

During the movement of joints 2, 4, and 6 simultaneously or separately, the arms are divided by joints and reassembled into rigid bodies. For example, when joints 2, 4, and 6 move simultaneously, the base and arm 1, arm 2 and arm 3, arm 4 and arm 5, arm 6, and end 7 are pairwise combined to form a multi-rigid body. To make $\boldsymbol{H}_{br}$ in Eq. (11) reversible, the space manipulator is reduced from 7-DOF to 3-DOF. As shown in Fig. 3, the joint numbers remain unchanged after reassembling the arm. The mass, joint vector, and centroid vector after the combination of rod $2i$ and rod $2i + 1$ are as follows:

https://doi.org/10.1017/S0263574723000747 Published online by Cambridge University Press

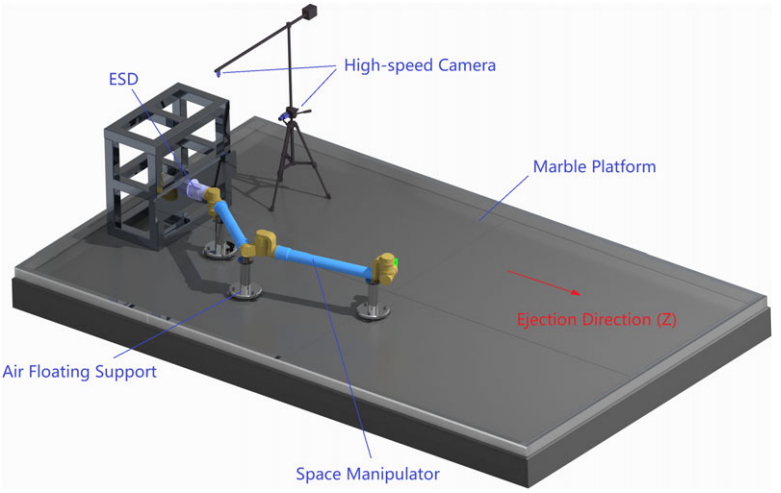


***Figure 2.*** *The layout of the plane ejection test of the manipulator.*

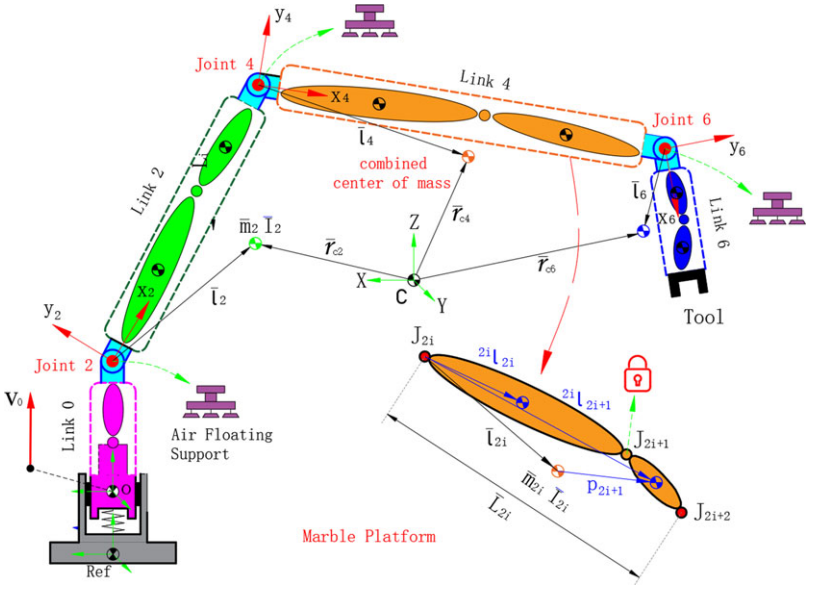


***Figure 3.*** *Robotic arm reconfiguration.*

$$\begin{aligned}
\bar{m}_{2i} &= m_{2i} + m_{2i+1} \\
\bar{\boldsymbol{L}}_{2i} &= \boldsymbol{L}_{2i} + \boldsymbol{L}_{2i+1} \\
\bar{\boldsymbol{l}}_{2i} &= \frac{m_{2i}{}^{2i}\boldsymbol{l}_{2i} + m_{2i+1}{}^{2i}_{2i+1}\boldsymbol{T}^{2i+1}\boldsymbol{l}_{2i+1}}{m_{2i} + m_{2i+1}}
\end{aligned} \tag{16}$$

$\bar{\boldsymbol{l}}_{2i}$ is the vector of the combined center of mass in the coordinates $2i$. ${}^{2i+1}\boldsymbol{l}_{2i+1}$ is the vector of the center of mass of the arm $2i+1$ in the original coordinates $2i+1$. Furthermore, the inertia tensor expressed in coordinates $2i$ of the combination of rod $2i$ and $2i+1$ at the combined center of mass $\bar{\boldsymbol{l}}_{2i}$ is as follows:

https://doi.org/10.1017/S0263574723000747 Published online by Cambridge University Press

$$\begin{aligned}\bar{\boldsymbol{I}}_{2i} &= {}^{2i}\boldsymbol{I}_{2i} + {}^{2i}\boldsymbol{I}_{2i+1} + \sum_{k=2i}^{2i+1}\left[m_k\left(\boldsymbol{P}_k^T\boldsymbol{P}_k\boldsymbol{E}_3 - \boldsymbol{P}_k\boldsymbol{P}_k^T\right)\right] \\ {}^{2i}\boldsymbol{I}_{2i+1} &= {}^{2i}_{2i+1}\boldsymbol{R}\cdot{}^{2i+1}\boldsymbol{I}_{2i+1}\cdot{}^{2i+1}\boldsymbol{R}^T\end{aligned} \tag{17}$$

where ${}^{2i}\boldsymbol{I}_{2i+1}$ is the inertia tensor consistent with the attitude of the coordinates $2i$ and located at the center of mass of the arm $2i+1$, and $\boldsymbol{P}_{2i+1} = {}^{2i}\boldsymbol{l}_{2i+1} - \bar{\boldsymbol{l}}_{2i}$.

The 7-DOF manipulator is simplified into a 3-DOF manipulator in a plane state with only four arms and three joints. Then, the combined center of mass and inertia tensor of the four arms are calculated according to Eqs. (16) and (17), and a new 3-DOF manipulator inertia matrix $\bar{\boldsymbol{H}}$ is reconstructed using the recursive formula [18–21]. The linear acceleration and angular acceleration of the manipulator with three degrees of freedom are further obtained from Eq. (1). In order to keep the number of joints 2, 4, and 6 unchanged, let $k = 2i = 2, 4, 6$:

$$\begin{aligned}{}^k\dot{\boldsymbol{\omega}}_k &= {}_{k-2}^{k}\boldsymbol{R}\left({}^{k-2}\dot{\boldsymbol{\omega}}_{k-2} + {}^{k-2}\boldsymbol{\omega}_{k-2}\times\dot{\boldsymbol{\theta}}_k{}^k\boldsymbol{Z}_k\right) + \ddot{\boldsymbol{\theta}}_k{}^k\boldsymbol{Z}_k \\ {}^k\dot{\boldsymbol{v}}_{c,k} &= {}^k\dot{\boldsymbol{v}}_k + {}^k\dot{\boldsymbol{\omega}}_k\times{}^k\bar{\boldsymbol{l}}_k + {}^k\boldsymbol{\omega}_k\times\left({}^k\boldsymbol{\omega}_k\times{}^k\bar{\boldsymbol{l}}_k\right)\end{aligned} \tag{18}$$

From Eq. (12), it is known that the DOF in five directions of the movable base is zero. Considering the reversibility of the matrix, the matrix is reduced from 13 × 13 to the 10 × 10 square matrix of the space state or the 4 × 4 square matrix $\bar{\boldsymbol{H}}$ of the plane state. By substituting Eq. (18) into recursive formula, the global inertia matrix $\bar{\boldsymbol{H}}$ in the plane state is obtained:

$$\bar{\boldsymbol{H}} = \begin{bmatrix} M & \sum\limits_{k=2,4,6}\bar{m}_k\boldsymbol{e}_z^T\bar{\boldsymbol{J}}_{vk} \\ \sum\limits_{k=2,4,6}\bar{m}_k\left(\boldsymbol{e}_z^T\bar{\boldsymbol{J}}_{vk}\right)^T & \sum\limits_{k=2,4,6}\left[\left(\bar{\boldsymbol{J}}_{\omega k}\right)^T\bar{\boldsymbol{I}}_k\bar{\boldsymbol{J}}_{\omega k} + \bar{m}_k(\bar{\boldsymbol{J}}_{v_k})^T\bar{\boldsymbol{J}}_{v_k}\right] \end{bmatrix} \tag{19}$$

Then brought into Eq. (15), the equivalent mass of the manipulator in the plane state is obtained.

## 3. Ejection calculation

The space manipulator ejection process is divided into three steps. In the first step, the manipulator is in the initial state, wherein the joint angular velocity, linear velocity, and angular velocity of the movable base are all zero. In the second step, the manipulator ejects in the ESD until the forces of springs decrease to zero (referred to as "zero force"). In the final step, the manipulator transits from a dynamic ejection having the relative rotation of joints to a stable ejection, where there is no relative rotation between the joints under the action of joint friction torque (referred to as "Stable Ejection").

The ESD consists of two springs with identical stiffness, represented by $k$ and $l$ for the stiffness and compression, respectively. The ejection process is a quarter cycle of simple harmonic vibration with a variable mass. During ejection, the manipulator's attitude and equivalent mass $m_{b,j}$ change with the angular variation of joints 2, 4, and 6. $m_{b,j}$ represents the equivalent mass of the $j$th calculation, and d $z_{f,j}$ represents the residual compression of the spring at the jth calculation when the manipulator is ejected inside ESD. $j$ is the number of calculation times, $f$ denotes ejected inside ESD, and $g$ denotes ejected outside ESD. The calculation algorithm flowchart in Fig. 5 is based on the ejection process in the three stages as shown in Fig. 4.

### *3.1. Ejection time*

The ejection process of the manipulator is regarded as the first quarter cycle of simple harmonic vibration with a variable mass, and the analytical solution is very complex to calculate the ejection velocity and joint angular variation [22]. As shown in Fig. 5, the ejection time can be obtained by the subsection superposition method. The whole ejection process is divided into $n$ segments, each with an ejection

https://doi.org/10.1017/S0263574723000747 Published online by Cambridge University Press

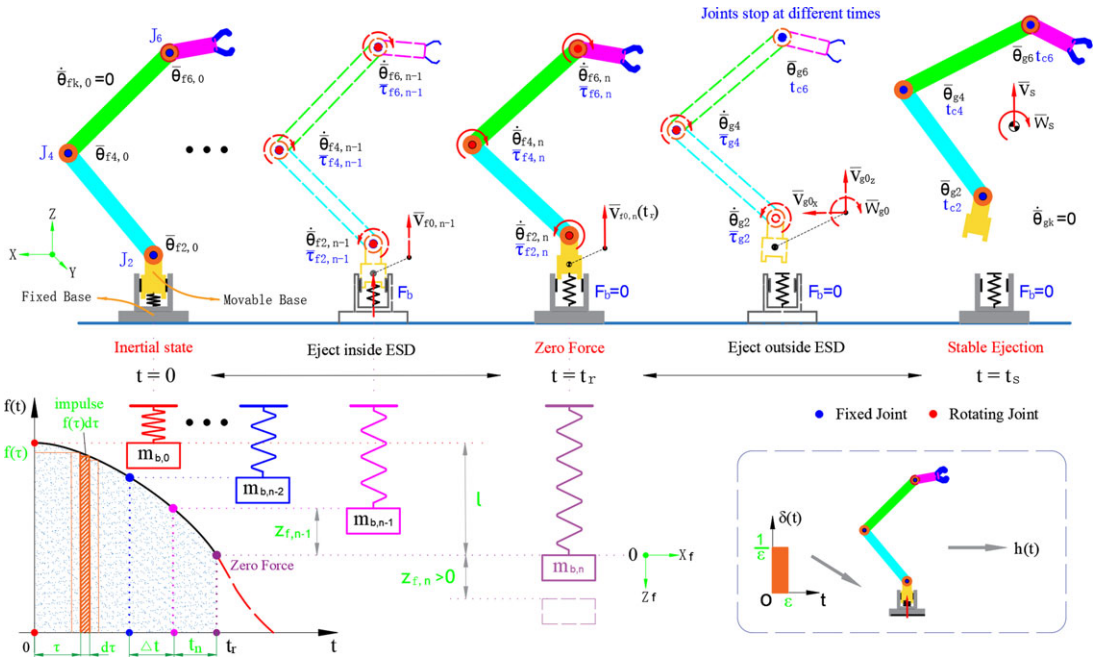


***Figure 4.*** *Three stages of ejection.*

time of $\Delta t = 0.02$ s. The spring recovery amount for each section is calculated based on the updated equivalent mass and then summed.

When the accumulative value $z_{f,j+1}$ exceeds zero, the recursive process reaches step $n$. To improve the accuracy of the result, the ejection time of the finial step $n$ is determined by the residual recovery amount of the spring and then added to the previous time, which is the zero force time $t_n = t_r$. During this process, the spring recovery force needs to be compensated due to the change in the vibration period:

Kinetic equation: $m_{b,j}\ddot{z}_{f,j} + kz_{f,j} = 0$

Initial condition: $z_{f,0} = -l, \dot{z}_{f,0} = 0, \omega_j = \sqrt{k/m_{b,j}}, t_0 = 0, \Delta t = 0.02, j = 0, 1, 2 \cdots n-1$

Recursive formula: $$z_{f,j+1} = z_{f,j}\cos(\omega_j \Delta t) + \frac{\dot{z}_{f,j}\sin(\omega_j \Delta t)}{\omega_j} \tag{20a}$$

$$\dot{z}_{f,j+1} = -z_{f,j}\omega_j \sin(\omega_j \Delta t) + \dot{z}_{f,j}\cos(\omega_j \Delta t) \tag{20b}$$

Judgment condition: if $z_{f,n} > 0$, then $$\Delta t_n = \frac{1}{\omega_{n-1}} \arcsin \frac{\omega_{n-1} z_{f,n-1}}{\sqrt{z_{f,n-1}^2 \omega_{n-1}^2 + \dot{z}_{f,n-1}^2}} \tag{20c}$$

Spring force compensation: $$F_{b,j+1} = kl\cos\omega_j t - kl\sum_{i=1}^{j}[\cos(\omega_i \cdot i\Delta t) - \cos(\omega_{i-1} \cdot i\Delta t)]$$

$$= kl(\cos\omega_j t - \Delta\psi_j) \tag{20d}$$

Ejection time: $$t_j = j\Delta t, t_n = (n-1)\Delta t + \Delta t_n \tag{20e}$$

https://doi.org/10.1017/S0263574723000747 Published online by Cambridge University Press

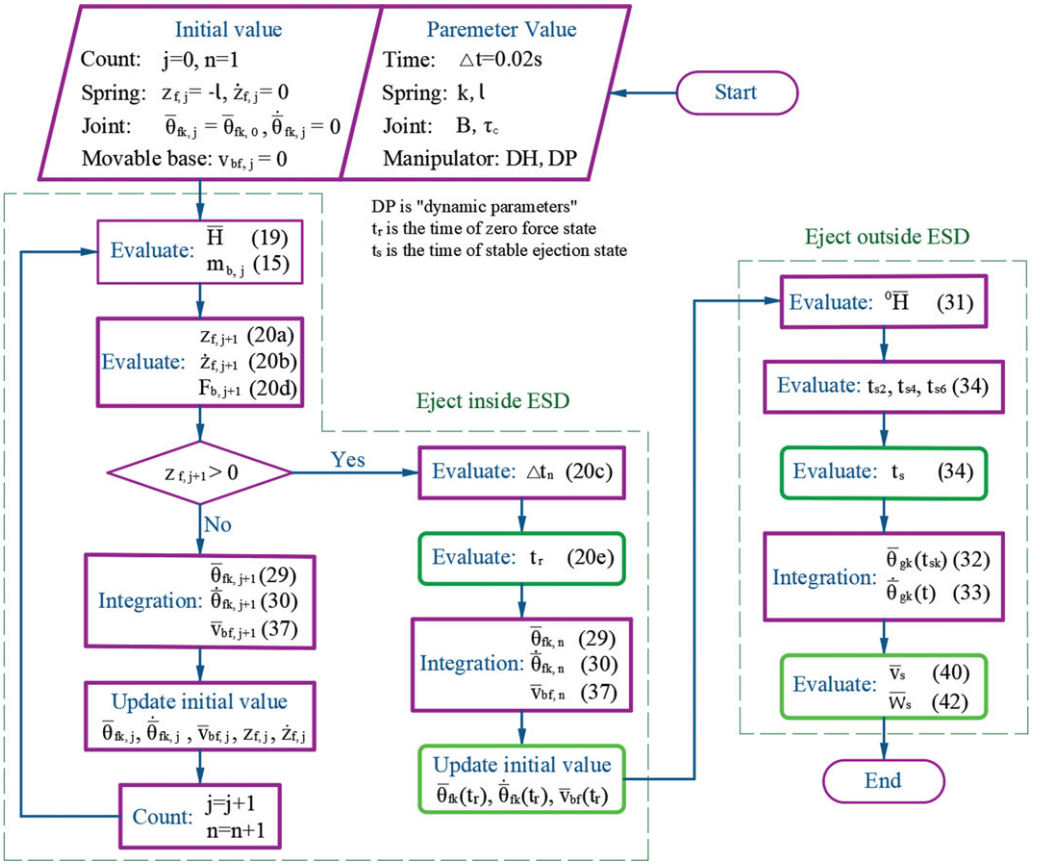


***Figure 5.*** *Flowchart of calculation algorithm.*

### *3.2. Joint angular variation*

In the process of the ejection, the spring force is parallel to the slide rail, and the manipulator moves along the smooth track without any relative rotation. Based on the force analysis, it is concluded that the external force acting on the manipulator is the spring force $F_b$, the normal force $F_n$ of the slide rail, and the moment $T_d$ acting on the slide rail. Since the manipulator has no displacement along the normal and torque rotation directions of the slide rail during ejection, the work done by $F_n$ and $T_d$ is zero.

In the case of manipulator ejection with a spring, the ejection time is generally 0.2–0.4 s. The motion equations can be modeled by Duhamel's integral, which can be summed up by the impulse response function. In the plane state, Eq. (10) can be rewritten as:

$$\begin{aligned} \bar{H}_b \ddot{\bar{x}}_0 + \bar{\boldsymbol{H}}_{br} \ddot{\bar{\boldsymbol{\theta}}} + \bar{c}_b &= F_b \\ \bar{\boldsymbol{H}}_{br}^T \ddot{\bar{x}}_0 + \bar{\boldsymbol{H}}_r \ddot{\bar{\boldsymbol{\theta}}} + \bar{\boldsymbol{c}}_r &= \bar{\boldsymbol{\tau}}_f \end{aligned} \tag{21}$$

The angular acceleration of the manipulator can be obtained by eliminating the variable $\ddot{\bar{x}}_0$ [23, 24]:

$$\ddot{\bar{\boldsymbol{\theta}}} = \hat{\boldsymbol{H}}_\theta^{-1} \left( \hat{\boldsymbol{J}}_\theta F_b + \hat{\boldsymbol{c}} - \bar{\boldsymbol{\tau}}_f \right) \tag{22}$$

where $\hat{\boldsymbol{H}}_\theta = \bar{\boldsymbol{H}}_{br}^T \bar{H}_b^{-1} \bar{\boldsymbol{H}}_{br} - \bar{\boldsymbol{H}}_r$, $\hat{\boldsymbol{J}}_\theta = \bar{\boldsymbol{H}}_{br}^T \bar{H}_b^{-1}$, $\hat{\boldsymbol{c}} = \bar{\boldsymbol{c}}_r - \bar{\boldsymbol{H}}_{br}^T \bar{H}_b^{-1} \bar{\boldsymbol{c}}_b$, and $\bar{H}_b^{-1} = 1/M$. The friction torque of the joint is composed of Coulomb friction $\bar{\tau}_c$ and joint damping $B$. Further, $\bar{\boldsymbol{\tau}}_s$ is static friction. When the manipulator is ejected, the spring force causes an additional torque on the joint, which needs enough torque to eject the multi-rigid body synchronously. However, the joint friction torque is limited,

https://doi.org/10.1017/S0263574723000747 Published online by Cambridge University Press

and when $\widehat{\boldsymbol{J}}_\theta F_b \le \bar{\boldsymbol{\tau}}_s$, the ejection passive torque is less than the joint static friction, so the joint does not rotate. Otherwise, it causes the joint to rotate. The friction torque of the joint can be expressed as:

$$\bar{\boldsymbol{\tau}}_f = \begin{cases} \widehat{\boldsymbol{J}}_\theta F_b & \widehat{\boldsymbol{J}}_\theta F_b \le \bar{\boldsymbol{\tau}}_s \\ \bar{\boldsymbol{\tau}}_c + B\dot{\bar{\boldsymbol{\theta}}} & \bar{\boldsymbol{J}}_\theta F_b > \bar{\boldsymbol{\tau}}_s, \dot{\bar{\boldsymbol{\theta}}} > 0 \\ -\bar{\boldsymbol{\tau}}_c + B\dot{\bar{\boldsymbol{\theta}}} & \widehat{\boldsymbol{J}}_\theta F_b > \bar{\boldsymbol{\tau}}_s, \dot{\bar{\boldsymbol{\theta}}} < 0 \end{cases} \tag{23}$$

Friction torque of each joint is $\bar{\boldsymbol{\tau}}_f = \begin{bmatrix} \bar{\tau}_{f2} & \bar{\tau}_{f4} & \bar{\tau}_{f6} \end{bmatrix}^T$, and $\bar{\boldsymbol{\tau}}_f$ are related to $\dot{\bar{\boldsymbol{\theta}}}$. The friction torque caused by ejection force is determined according to Eq. (23). And $\bar{\boldsymbol{\tau}}_f$ is determined according to the direction of $\dot{\bar{\boldsymbol{\theta}}}$. In a very short period of time, the velocity-dependent term $\widehat{\boldsymbol{c}}$ can be ignored. When $\dot{\bar{\boldsymbol{\theta}}} > 0$, Eq. (22) can be expressed as follows (when $\dot{\bar{\boldsymbol{\theta}}} < 0$, the following $\bar{\boldsymbol{\tau}}_c$ takes a minus sign):

$$\ddot{\bar{\boldsymbol{\theta}}} + \widehat{\boldsymbol{H}}_\theta^{-1} B\dot{\bar{\boldsymbol{\theta}}} = \widehat{\boldsymbol{H}}_\theta^{-1}\widehat{\boldsymbol{J}}_\theta F_b - \widehat{\boldsymbol{H}}_\theta^{-1}\bar{\boldsymbol{\tau}}_c \tag{24}$$

Then calculate the unit impulse response function at zero initial state $h(t)$:

$$\begin{aligned} &\ddot{\boldsymbol{h}}(t) + \hat{\boldsymbol{H}}_\theta^{-1} B\dot{\boldsymbol{h}}(t) = \boldsymbol{\delta}(t) \\ &\boldsymbol{h}(0^-) = 0, \quad \dot{\boldsymbol{h}}(0^-) = \begin{bmatrix} 0 & 0 & 0 \end{bmatrix} \end{aligned} \tag{25}$$

Since the impulse is applied to the system in an infinitely short time, the displacement remains unchanged. When the velocity jumps from $0^-$ to $0^+$, the acceleration can produce an instantaneous pulse $\boldsymbol{\delta}(t)$. After the impulse, the system is in free vibration mode, so the above equation is equivalent to:

$$\begin{aligned} &\ddot{\boldsymbol{h}}(t) + \hat{\boldsymbol{H}}_\theta^{-1} B\dot{\boldsymbol{h}}(t) = 0 \\ &\boldsymbol{h}(0^+) = 0, \quad \dot{\boldsymbol{h}}(0^+) = \begin{bmatrix} 1 & 1 & 1 \end{bmatrix} \end{aligned} \tag{26}$$

The unit impulse response function $\boldsymbol{h}(t)$ can be obtained by solving Eq. (26):

$$\boldsymbol{h}(t) = \frac{1}{\boldsymbol{H}_\theta^{-1} B}\left(1 - e^{-\hat{\boldsymbol{H}}_\theta^{-1} Bt}\right) \quad t \ge 0 \tag{27}$$

As shown in Fig. 4, when $t \in [0, t_r]$, Duhamel's integral is used to calculate the cumulative impulse response function of excitation $\boldsymbol{f}(t) = \widehat{\boldsymbol{H}}_\theta^{-1}\widehat{\boldsymbol{J}}_\theta F_b - \widehat{\boldsymbol{H}}_\theta^{-1}\bar{\boldsymbol{\tau}}_c$. $\bar{\boldsymbol{\theta}}_{f,\text{initial}}$ is the response caused by the initial condition at time $t_j$. The joint angle is as follows:

$$\begin{aligned} \bar{\boldsymbol{\theta}}_{f,j+1} &= \bar{\boldsymbol{\theta}}_{f,\text{initial}} + \int_{t_j}^{t_{j+1}} \boldsymbol{h}(t_{j+1} - \tau)\boldsymbol{f}(\tau) d\tau \\ &= \bar{\boldsymbol{\theta}}_{f,\text{initial}} + \frac{1}{\boldsymbol{\beta}_\theta}\int_{t_j}^{t_{j+1}} \left[1 - e^{-\boldsymbol{\beta}_\theta \cdot (t_{j+1} - \tau)}\right]\left[\boldsymbol{\zeta}_\theta \cos(\omega_j \tau) - \boldsymbol{\zeta}_\theta \Delta\psi_j - \boldsymbol{\gamma}_\theta\right] d\tau \end{aligned} \tag{28}$$

where $\boldsymbol{\zeta}_\theta = \widehat{\boldsymbol{H}}_\theta^{-1}\widehat{\boldsymbol{J}}_\theta \cdot kl$, $\boldsymbol{\beta}_\theta = \widehat{\boldsymbol{H}}_\theta^{-1} B$, and $\boldsymbol{\gamma}_\theta = \hat{\boldsymbol{H}}_\theta^{-1}\bar{\boldsymbol{\tau}}_c$. Duhamel's integral is obtained under zero initial conditions, and the full response of the system also includes the part of the response caused by the initial conditions. The manipulator is in static state before ejection, so the initial angle of the joint is $\bar{\boldsymbol{\theta}}_{f,0} = \begin{bmatrix} \bar{\theta}_{f2,0} & \bar{\theta}_{f4,0} & \bar{\theta}_{f6,0} \end{bmatrix}$. The initial angular velocity is $\dot{\bar{\boldsymbol{\theta}}}_{f,0} = \begin{bmatrix} \dot{\bar{\theta}}_{f2,0} & \dot{\bar{\theta}}_{f4,0} & \dot{\bar{\theta}}_{f6,0} \end{bmatrix}$.

The ejection process is divided into two stages. One is ejected inside ESD, where the movable base is limited by boundary conditions Eq. (12). The other is ejected outside ESD, where the movable base has no constraints. It is necessary to calculate the joint angular variation under the two states, respectively.

### *3.2.1. Eject inside ESD*

During ejection in ESD, the full expression of the joint angle $\bar{\boldsymbol{\theta}}_{f,j} = \begin{bmatrix} \bar{\theta}_{f2,j} & \bar{\theta}_{f4,j} & \bar{\theta}_{f6,j} \end{bmatrix}$ under the spring recovery force and the initial response is as follows. $\bar{\theta}_{fk,j}$ denotes the $j$th calculation of the angle of joint

https://doi.org/10.1017/S0263574723000747 Published online by Cambridge University Press

$k$ when the manipulator is ejected inside ESD:

$$\begin{aligned}\bar{\theta}_{fk,j+1} = \bar{\theta}_{fk,j} + \frac{\dot{\bar{\theta}}_{fk,j}}{\beta_{\theta k}}\left(1 - e^{\beta_{\theta k}(t_j - t_{j+1})}\right) - \frac{\zeta_{\theta k}\Delta\psi_j + \gamma_{\theta k}}{\beta_{\theta k}}\left[t_{j+1} - t_j - \frac{1 - e^{\beta_{\theta k}(t_j - t_{j+1})}}{\beta_{\theta k}}\right] \\ + \frac{\zeta_{\theta k}}{\omega_j^2 + \beta_{\theta k}^2}\left\{\frac{\beta_{\theta k}}{\omega_j}\sin(\omega_j t_{j+1}) + e^{\beta_{\theta k}(t_j - t_{j+1})}\cos(\omega_j t_j) - \cos(\omega_j t_{j+1})\right. \\ \left. + \frac{\omega_j^2\left[e^{\beta_{\theta k}(t_j - t_{j+1})} - 1\right] - \beta_{\theta k}^2}{\omega_j \beta_{\theta k}}\sin(\omega_j t_j)\right\}\end{aligned} \tag{29}$$

where $\dot{\bar{\theta}}_{fk,j}$ denotes the $j$th calculation of the angular velocity of joint $k$ when the manipulator is ejected inside ESD. So the angular velocity is

$$\begin{aligned}\dot{\bar{\theta}}_{fk,j+1} = \dot{\bar{\theta}}_{fk,j} e^{\beta_{\theta k}(t_j - t_{j+1})} - \frac{\zeta_{\theta k}\Delta\psi_j + \gamma_{\theta k}}{\beta_{\theta k}}\left[1 - e^{\beta_{\theta k}(t_j - t_{j+1})}\right] + \frac{\zeta_{\theta k}}{\omega_j^2 + \beta_{\theta k}^2}\left\{\omega_j \sin(\omega_j t_{j+1})\right. \\ \left. + \beta_{\theta k}\cos(\omega_j t_{j+1}) - \beta_{\theta k} e^{\beta_{\theta k}(t_j - t_{j+1})}\cos(\omega_j t_j) - \omega_j e^{\beta_{\theta k}(t_j - t_{j+1})}\sin(\omega_j t_j)\right\}\end{aligned} \tag{30}$$

### *3.2.2. Eject outside ESD*

Upon ejection outside ESD, the manipulator is devoid of any external forces except for internal forces arising from joint friction, as the spring force $F_b$ reduces to zero. Since it is no longer constrained by ESD, the boundary condition Eq. (12) becomes $v_x = v_z \neq 0, \omega_y \neq 0, v_y = \omega_x = \omega_z = 0$. Considering the reversibility of the inertia matrix, it becomes a $6 \times 6$ square matrix ${}^o\bar{\boldsymbol{H}}$ in a plane state:

$$\begin{bmatrix} \boldsymbol{M}\boldsymbol{E}_{xz}^T\boldsymbol{E}_{xz} & \boldsymbol{M}\boldsymbol{E}_{xz}^T\left(\bar{\boldsymbol{r}}_{oc}^*\right)^T\boldsymbol{e}_y & \sum_{k=2}^{6}\bar{m}_k\boldsymbol{E}_{xz}^T\bar{\boldsymbol{J}}_{vk} \\ \boldsymbol{M}\boldsymbol{e}_y^T\bar{\boldsymbol{r}}_{oc}^*\boldsymbol{E}_{xz} & \sum_{k=0}^{6}\boldsymbol{e}_y^T\left[\bar{\boldsymbol{I}}_k + \bar{m}_k\left(\bar{\boldsymbol{r}}_{ok}^*\right)^T\bar{\boldsymbol{r}}_{ok}^*\right]\boldsymbol{e}_y & \sum_{k=2}^{6}\boldsymbol{e}_y^T\left[\bar{\boldsymbol{I}}_k\bar{\boldsymbol{J}}_{\omega k} - \bar{m}_k\left(\bar{\boldsymbol{r}}_{ok}^*\right)^T\bar{\boldsymbol{J}}_{vk}\right] \\ \sum_{k=2}^{6}\bar{m}_k\left(\bar{\boldsymbol{J}}_{vk}\right)^T\boldsymbol{E}_{xz} & \sum_{k=2}^{6}\left[\left(\bar{\boldsymbol{J}}_{\omega k}\right)^T\bar{\boldsymbol{I}}_k - \bar{m}_k\left(\bar{\boldsymbol{J}}_{vk}\right)^T\bar{\boldsymbol{r}}_{ok}^*\right]\boldsymbol{e}_y & \sum_{k=2}^{6}\left[\left(\bar{\boldsymbol{J}}_{\omega k}\right)^T\bar{\boldsymbol{I}}_k\bar{\boldsymbol{J}}_{\omega k} + \bar{m}_k\left(\bar{\boldsymbol{J}}_{vk}\right)^T\bar{\boldsymbol{J}}_{vk}\right] \end{bmatrix} \tag{31}$$

where $\boldsymbol{E}_{xz} = \begin{bmatrix} 1 & 0 & 0 \\ 0 & 0 & 1 \end{bmatrix}^T$, $\boldsymbol{e}_y = \begin{bmatrix} 0 & 1 & 0 \end{bmatrix}^T$, and ${}^0\boldsymbol{\zeta}_\theta = {}^0\boldsymbol{H}_\theta^{-1}{}^0\widehat{\boldsymbol{J}}_\theta \cdot kl$, ${}^0\boldsymbol{\beta}_\theta = {}^0\widehat{\boldsymbol{H}}_\theta^{-1}B$, ${}^0\boldsymbol{\gamma}_\theta = {}^0\widehat{\boldsymbol{H}}_\theta^{-1}\bar{\boldsymbol{\tau}}_c$.

The initial joint conditions are the joint angle $\bar{\theta}_{fk}(t_r)$ and the joint angular velocity $\dot{\bar{\theta}}_{fk}(t_r)$. The joint will continue to rotate under the initial conditions and gradually stop rotating under the action of joint friction torque. Since joints stop at different times, it causes the change of the inertia tensor $\boldsymbol{I}_k$ of the arm and the inertia matrix ${}^m\bar{\boldsymbol{H}}$, $m = 0, 1, 2, 3$ of the manipulator, as shown in Fig. 6. Considering that the joint is greatly influenced by friction, and the effect of inertia change is small, so the effect of ${}^m\bar{\boldsymbol{H}}$ change is ignored here. $\bar{\theta}_{gk}$ denotes the angle of joint $k$ when the manipulator is ejected outside ESD:

$$\bar{\theta}_{gk}(t) = \bar{\theta}_{fk}(t_r) + \left(\frac{\dot{\bar{\theta}}_{fk}(t_r)}{{}^0\beta_{\theta k}} + \frac{{}^0\gamma_{\theta k}}{{}^0\beta_{\theta k}^2}\right)\left[1 - e^{-{}^0\beta_{\theta k}(t - t_r)}\right] - \frac{{}^0\gamma_{\theta k}}{{}^0\beta_{\theta k}}(t - t_r) \tag{32}$$

where $\dot{\bar{\theta}}_{gk}$ denotes the angular velocity of joint $k$ when the manipulator is ejected outside ESD:

$$\dot{\bar{\theta}}_{gk}(t) = \left[\dot{\bar{\theta}}_{fk}(t_r) + \frac{{}^0\gamma_{\theta k}}{{}^0\beta_{\theta k}}\right]e^{-{}^0\beta_{\theta k}(t - t_r)} - \frac{{}^0\gamma_{\theta k}}{{}^0\beta_{\theta k}} \tag{33}$$

When the angular velocity of all joints gradually decreases to zero, the joints of the manipulator stop rotating. The whole manipulator then ejects at the same velocity, and the attitude does not change. This

https://doi.org/10.1017/S0263574723000747 Published online by Cambridge University Press

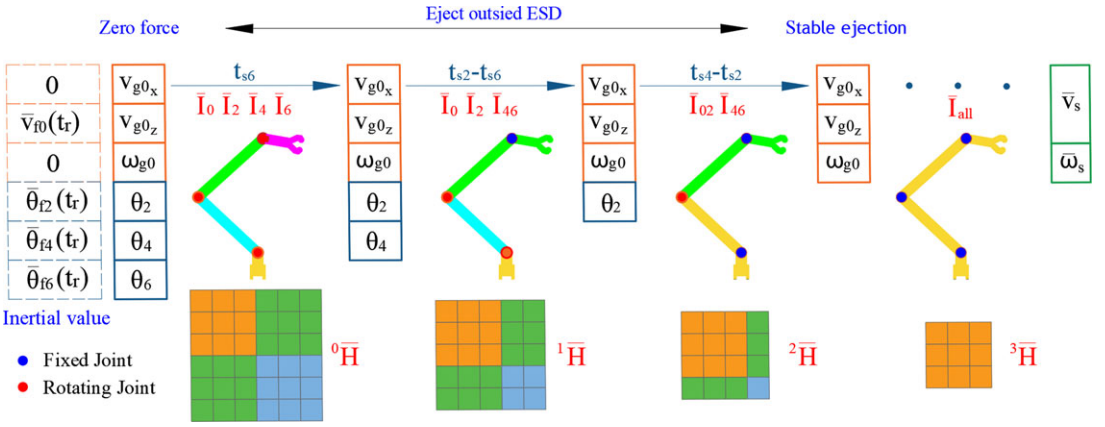


***Figure 6.*** *Status of the manipulator when it is ejected outside ESD.*

is the stable time $t_s$, and $\dot{\bar{\theta}}_{gk}(t_s) = 0$:

$$t_s = \max\{t_{s2}, t_{s4}, t_{s6}\} = \max\left\{\frac{1}{{}^0\beta_{\theta k}} \ln\left(\frac{\dot{\bar{\theta}}_{fk}(t_r)^0 \beta_{\theta k} + {}^0\gamma_{\theta k}}{{}^0\gamma_{\theta k}}\right) + t_r\right\} \quad k = 2, 4, 6 \tag{34}$$

Assuming that $t_{s6} = \min\{t_{s2}, t_{s4}, t_{s6}\}$ and $t_{s4} = \max\{t_{s2}, t_{s4}, t_{s6}\}$, it may be different in other cases.

### *3.3. Ejection velocity*

The acceleration of the movable base can be obtained by eliminating the variable $\ddot{\bar{\boldsymbol{\theta}}}$ from Eq. (21):

$$\ddot{\bar{x}}_0 = \widehat{\boldsymbol{H}}_b^{-1}\widehat{\boldsymbol{J}}_b F_b - \widehat{\boldsymbol{H}}_b^{-1}\left(\bar{\boldsymbol{\tau}}_c + B\dot{\bar{\boldsymbol{\theta}}}\right) \tag{35}$$

where $\widehat{\boldsymbol{H}}_b = \bar{\boldsymbol{H}}_r \bar{\boldsymbol{H}}_{br}^{-1} \bar{H}_b - \bar{\boldsymbol{H}}_{br}^T$ and $\widehat{\boldsymbol{J}}_b = \bar{\boldsymbol{H}}_r \bar{\boldsymbol{H}}_{br}^{-1}$. Unlike Eq. (24), we can integrate both sides of Eq. (35) directly to obtain the ejection velocity $\bar{v}_0(t)$ of the movable base, as we have already calculated the angular velocity of the joint.

#### *3.3.1. Eject inside ESD*

In the initial condition $\dot{\bar{x}}_{f0} = \bar{v}_{f0}(0) = 0$, $\bar{v}_{f0}$ denotes the ejection velocity of the movable base when the manipulator is ejected inside ESD. By substituting $\bar{\boldsymbol{\theta}}_f(t)$ with $\bar{\boldsymbol{\theta}}(t)$, the following equation takes into account the energy loss caused by joint friction $\bar{\boldsymbol{\tau}}_c$ and damping $B$ in the ejection process:

$$\int_{t_j}^{t_{j+1}} \ddot{\bar{x}}_{f0} dt = \widehat{\boldsymbol{H}}_b^{-1}\widehat{\boldsymbol{J}}_b kl \int_{t_j}^{t_{j+1}} \left[\cos(\omega_j t) - \Delta\psi_j\right] dt - \int_{t_j}^{t_{j+1}} \widehat{\boldsymbol{H}}_b^{-1}\left(\bar{\boldsymbol{\tau}}_c + B\dot{\bar{\boldsymbol{\theta}}}_{fj}\right) dt \tag{36}$$

where $\zeta_b = \widehat{\boldsymbol{H}}_b^{-1}\widehat{\boldsymbol{J}}_b kl$, $\boldsymbol{\beta}_b = \widehat{\boldsymbol{H}}_b^{-1} B$, $\gamma_b = \widehat{\boldsymbol{H}}_b^{-1}\bar{\boldsymbol{\tau}}_c$. We have the following equation:

$$\bar{v}_{f0,j+1} = \bar{v}_{f0,j} + \frac{\zeta_b}{\omega_j}\left[\sin(\omega_j t_{j+1}) - \sin(\omega_j t_j)\right] - \left(\zeta_b \Delta\psi_j + \gamma_b\right)\left(t_{j+1} - t_j\right) - \boldsymbol{\beta}_b\left[\bar{\boldsymbol{\theta}}_{f,j+1} - \bar{\boldsymbol{\theta}}_{fj}\right] \tag{37}$$

The ejection velocity of the movable base can be obtained by solving Eq. (37) with $\bar{\boldsymbol{\theta}}_{f,j+1}(t)$ from Eq. (29) substituted. At $t_n = t_r$, the velocity $\bar{v}_{f0}(t_r)$ represents the ejection velocity of the movable base at zero force separation.

https://doi.org/10.1017/S0263574723000747 Published online by Cambridge University Press

### *3.3.2. Eject outside ESD*

When the manipulator is ejected outside ESD, the force $F_b$ is zero, and each joint gradually stops under the influence of joint friction torque $\bar{\tau}_f$. At time $t_s$, the angular velocity of all joints reduces to zero, resulting in no change in the velocity of the movable base, and the entire manipulator ejects at a constant velocity $\bar{v}_s$. Integrating both sides of Eq. (35) with $F_b = 0$, we have

$$\int_{t_r}^{t} \ddot{\bar{\boldsymbol{x}}}_{g0} dt = -\int_{t_r}^{t} {}^{m}\widehat{\boldsymbol{H}}_b^{-1}\left({}^{m}\bar{\boldsymbol{\tau}}_c + B^{m}\dot{\bar{\boldsymbol{\theta}}}_g\right) dt \tag{38}$$

where $\dot{\bar{\boldsymbol{x}}}_{g0} = \bar{\boldsymbol{v}}_{g0} = \begin{bmatrix} \bar{v}_{g0_x} & \bar{v}_{g0_z} & \bar{\omega}_{g0} \end{bmatrix}^T$, $m$ is in the upper left corner of ${}^{m}\bar{\boldsymbol{\tau}}_c$, and ${}^{m}\dot{\bar{\boldsymbol{\theta}}}_g$ denotes the number of elements in a vector. When $m = 0, 1, 2, 3$, the number of elements is $3, 2, 1, 0$.

$\bar{\boldsymbol{v}}_{g0}$ includes the ejection velocity and ejection angular velocity of the movable base when the manipulator is ejected outside ESD. Assuming that the joints stop in the sequence depicted in Fig. 6, and $t_2 < t < t_4$, then Eq. (38) becomes

$$\begin{aligned} \bar{\boldsymbol{v}}_{g0}(t) = \bar{\boldsymbol{v}}_{f0}(t_r) &- {}^{0}\widehat{\boldsymbol{H}}_b^{-1}{}^{0}\bar{\boldsymbol{\tau}}_c(t_{s6} - t_r) - {}^{1}\widehat{\boldsymbol{H}}_b^{-1}{}^{1}\bar{\boldsymbol{\tau}}_c(t_{s2} - t_{s6}) - {}^{2}\widehat{\boldsymbol{H}}_b^{-1}{}^{2}\bar{\boldsymbol{\tau}}_c(t - t_{s2}) \\ &- {}^{0}\widehat{\boldsymbol{H}}_b^{-1}B\left[{}^{0}\bar{\boldsymbol{\theta}}_g(t_{s6}) - {}^{0}\bar{\boldsymbol{\theta}}_g(t_r)\right] - {}^{1}\widehat{\boldsymbol{H}}_b^{-1}B\left[{}^{1}\bar{\boldsymbol{\theta}}_g(t_{s2}) - {}^{1}\bar{\boldsymbol{\theta}}_g(t_{s6})\right] \\ &- {}^{2}\widehat{\boldsymbol{H}}_b^{-1}B\left[{}^{2}\bar{\boldsymbol{\theta}}_g(t) - {}^{2}\bar{\boldsymbol{\theta}}_g(t_{s2})\right] \end{aligned} \tag{39}$$

For simplicity, the ejection velocity $\bar{v}_s$ at the stable stage can be calculated by the method of energy conservation. The spring potential energy is equal to the sum of the linear velocity kinetic energy $T_v$, angular velocity energy $T_\omega$, and joint energy loss $\eta$ of the manipulator:

$$\begin{aligned} \bar{v}_s &= \sqrt{\frac{kl^2 - \bar{\omega}_s^2 \bar{I}_{\text{all}} - 2\eta}{M}} \\ \eta &= \sum_{k=2,4,6}\left(\int_{\bar{\theta}_{fk,0}}^{\bar{\theta}_{gk}} \bar{\tau}_f d\theta\right) = \sum_{k=2,4,6}\left[\int_{0}^{t_r}\left(\bar{\tau}_{ck} + B\dot{\bar{\theta}}_{fk}\right)\dot{\bar{\theta}}_{fk} dt + \int_{t_r}^{t_{sk}}\left(\bar{\tau}_{ck} + B\dot{\bar{\theta}}_{gk}\right)\dot{\bar{\theta}}_{gk} dt\right] \end{aligned} \tag{40}$$

where $\boldsymbol{I}_{\text{all}}$ is the global inertia tensor of the manipulator in a certain attitude when all the joints are fixed. The value of $\bar{\omega}_s$ can be obtained by Eq. (42), which is derived by substituting Eqs. (29)–(33) into Eq. (40). After stable ejection, the velocity of the manipulator remains constant since the arm is not subjected to external forces.

## *3.4. Ejection angular velocity*

The manipulator is guided by the slide rail when ejected from the ESD; thus, no angular velocity is generated. After disengaging from the ESD, the external force and torque on the manipulator become zero. However, due to the relative rotation of the joints, the velocities of different rigid bodies are not the same initially. After ejecting from the ESD for some time, the velocity of the multi-rigid body becomes the same as the velocity of the center of mass under the effects of internal forces [25].

According to the theorem of the moment of momentum, when the external torque is zero, the moment of multi-rigid bodies at the center of mass is conserved from the separation time to the stable time. After the ejection becomes stable, the joints of the manipulator stop rotating, and the whole manipulator ejects at the same ejection velocity and angular velocity. Then the ejection angular velocity $\boldsymbol{\omega}_s$ of the manipulator can be obtained as follows:

$$\sum_{i=0}^{7}\left[\boldsymbol{I}_i\boldsymbol{\omega}_i + m_i\boldsymbol{r}_{ci} \times \boldsymbol{v}_{ci}\right] = \boldsymbol{I}_{\text{all}}\boldsymbol{\omega}_s \tag{41}$$

The left side of the equation is the moment of momentum of each arm of the manipulator relative to the center of mass of the manipulator when the manipulator just ejects from the ESD. The right side is the

https://doi.org/10.1017/S0263574723000747 Published online by Cambridge University Press

***Table I.*** *Dynamic parameters of the manipulator with air-floating support.*

| $i$ | $\alpha_{i-1}$ | $\alpha_{i-1}$ | $d_i$ | $\theta_i$ | **Angle** |
|---|---|---|---|---|---|
| 1 | 0° | 0 | 250 | 0° | [−180°180°] |
| 2 | 90° | 0 | 0 | 180° | [−90°90°] |
| 3 | 90° | 0 | 1800 | 180° | [−180°180°] |
| 4 | 90° | 150 | 0 | 180° | [−180°0°] |
| 5 | 90° | 0 | 2280 | 180° | [−180°180°] |
| 6 | 90° | 0 | 0 | 180° | [−90°90°] |
| 7 | 90° | 280 | 0 | 180° | [−180°180°] |

moment of momentum of each arm of the manipulator relative to the center of mass of the manipulator after the steady state (when each joint has no relative rotation).

Where $\bar{\omega}_{f0}(t_r) = 0$ and $\dot{\bar{\theta}}_{fk}$ is the angular velocity of the arm $k$ at the zero force time $t_r$, which is obtained from Eq. (30), and $\bar{\boldsymbol{v}}_{ck}$ is the absolute velocity of the center of mass of the arm $k$ in the coordinates of the center of mass of the manipulator at the time of separation, which can be obtained by replacing Eqs. (30) and (37) into Eq. (1). After transforming into a plane state, the ejection angular velocity $\bar{\boldsymbol{\omega}}_s$ of the manipulator can be obtained as follows:

$$\bar{\boldsymbol{\omega}}_s = \frac{\sum\limits_{k=2,4,6}\left[\bar{\boldsymbol{I}}_k \cdot \dot{\bar{\theta}}_{fk}(t_r)\boldsymbol{e}_y + \bar{m}_k\bar{\boldsymbol{r}}_{ck} \times \bar{\boldsymbol{v}}_{ck}\right] + \bar{m}_0\bar{\boldsymbol{r}}_{c0} \times \bar{v}_{f0}(t_r)\boldsymbol{e}_z}{\bar{\boldsymbol{I}}_{\text{all}}} \tag{42}$$

## 4. Ejection simulation verification

The space manipulator is a 7-DOF manipulator with several typical attitudes while in orbit. It is necessary for the manipulator to not interfere with the surrounding spacecraft when being ejected in a certain attitude. Regardless of the attitudes, the ejection direction is always along the Z direction. Five typical attitudes are considered to analyze the equivalent mass of the manipulator along the Z direction.

### *4.1. Simulation model parameters*

The DH parameters of the space manipulator are shown in Table I. The manipulator used in the plane ejection test is ejected together with the air-floating support, and the dynamic parameters of the manipulator and the air-floating support are shown in Table II. The static friction torque of joint $\tau_s = 4$ Nm and Coulomb friction torque of joint $\tau_c = 2$ Nm. Spring stiffness $k = 812.7$ N/m, working compression $l = 86$ mm. After the joint damping is corrected in Section 5.2, the final value is $B = 5.4$ Nms/rad.

Based on the manipulator used in the plane ejection test, the theoretical and the simulation models are transformed into the plane state. During the plane transformation, only joints 1, 3, 5, and 7 need to be fixed to their initial angles, while joints 2, 4, and 6 rotate. Then the theoretical calculation, simulation, and experimental verification of plane ejection are compared with five typical of attitude, which can be extended to any attitude in space.

### *4.2. MATLAB and ADAMS simulation*

The monitoring point of MATLAB theoretical calculation and ADAMS simulation is the origin of the movable base coordinate O, which is considered the extraction point of the ejection velocity and angular velocity of the manipulator. The theoretical calculation and simulation results in Table III are obtained using the parameters in Table I and Table II. Adams simulation results are shown in Fig. 7.

https://doi.org/10.1017/S0263574723000747 Published online by Cambridge University Press

***Table II.*** *Dynamic parameters of the manipulator with air-floating support.*

| | Centroid (mm) | | | | Inertia relative to centroid C (kg∗mm$^2$) | | | | | |
|---|---|---|---|---|---|---|---|---|---|---|
| **Arm** | ***X*** | ***Y*** | ***Z*** | **Mass (kg)** | $I_{xx}$ | $I_{yy}$ | $I_{zz}$ | $I_{xy}$ | $I_{xz}$ | $I_{yz}$ |
| Base | 0 | 0 | 0 | 6.528 | 8.70e + 3 | 8.71e + 3 | 7.29e + 3 | 82.8 | 0 | 60.4 |
| Link1 | 0 | 17.5 | −29.45 | 8.986 | 8.69e + 3 | 7.60e + 3 | 6.34e + 3 | 0 | −1.40e + 3 | 0 |
| Link2 | −1.65 | −573.77 | −16.18 | 34.83 | 2.00e + 6 | 1.12e + 5 | 1.96e + 6 | −4.47e + 3 | 1.41e + 5 | 6.60e + 2 |
| Link3 | 31.13 | 8.75 | −27.84 | 19.44 | 4.11e + 4 | 8.63e + 4 | 1.01e + 5 | −1.80e + 4 | −4.25e + 3 | −1.39e + 4 |
| Link4 | 1.09 | −181.88 | −64.95 | 4.28 | 3.30e + 4 | 1.93e + 4 | 2.12e + 4 | −2.99e + 2 | 1.24e + 4 | 2.71e + 2 |
| Link5 | −1.17 | 64.86 | −403.95 | 14.18 | 1.99e + 6 | 1.94e + 6 | 9.08e + 4 | −6.71e + 2 | −2.11e + 5 | 1.33e + 3 |
| Link6 | −0.12 | −39.04 | −2.07 | 18.86 | 3.32e + 4 | 3.84e + 4 | 2.86e + 4 | 28.71 | 2.67e + 3 | −112.73 |
| Link7 | 0.128 | −26.98 | 173.13 | 9.795 | 5.69e + 4 | 4.29e + 4 | 3.32e + 4 | −48.42 | 5.51e + 2 | −42.55 |

***Table III.*** *Ejection calculation and simulation results of the manipulator in plane air flotation.*

| | **Effective mass (kg)** | | | **Ejection time (s)** | | **Ejection velocity (mm/s)** | | | **Joint angular variance (°)** | | | |
|---|---|---|---|---|---|---|---|---|---|---|---|---|
| **Attitude** | **Space** | **Plane** | **Joint 4 free** | **Theory** | **simulation** | **Theory** | **simulation** | **Angular velocity (°/s)** | **Joint 2 simulation** | **Joint 2 theory** | **Joint 4 simulation** | **Joint 4 theory** |
| 1 | 26.93 | 48.73 | 53.47 | 0.272 | 0.275 | 478.1 | 463.1 | −9.45 | −0.67 | −0.75 | −4.20 | −4.36 |
| 2 | 21.89 | 33.05 | 83.74 | 0.225 | 0.230 | 573.8 | 564.7 | 4.95 | −4.36 | −4.48 | −6.61 | −6.75 |
| 3 | 19.06 | 33.76 | 53.45 | 0.228 | 0.234 | 562.5 | 546.3 | −4.82 | −2.63 | −2.68 | −4.39 | −4.57 |
| 4 | 25.31 | 44.95 | 56.47 | 0.261 | 0.265 | 494.4 | 489.6 | −13.4 | 1.41 | 1.48 | −1.73 | −1.63 |
| 5 | 48.73 | 84.87 | 85.91 | 0.359 | 0.352 | 377.2 | 370.3 | −0.72 | 0.14 | 0.22 | 0.16 | 0.28 |

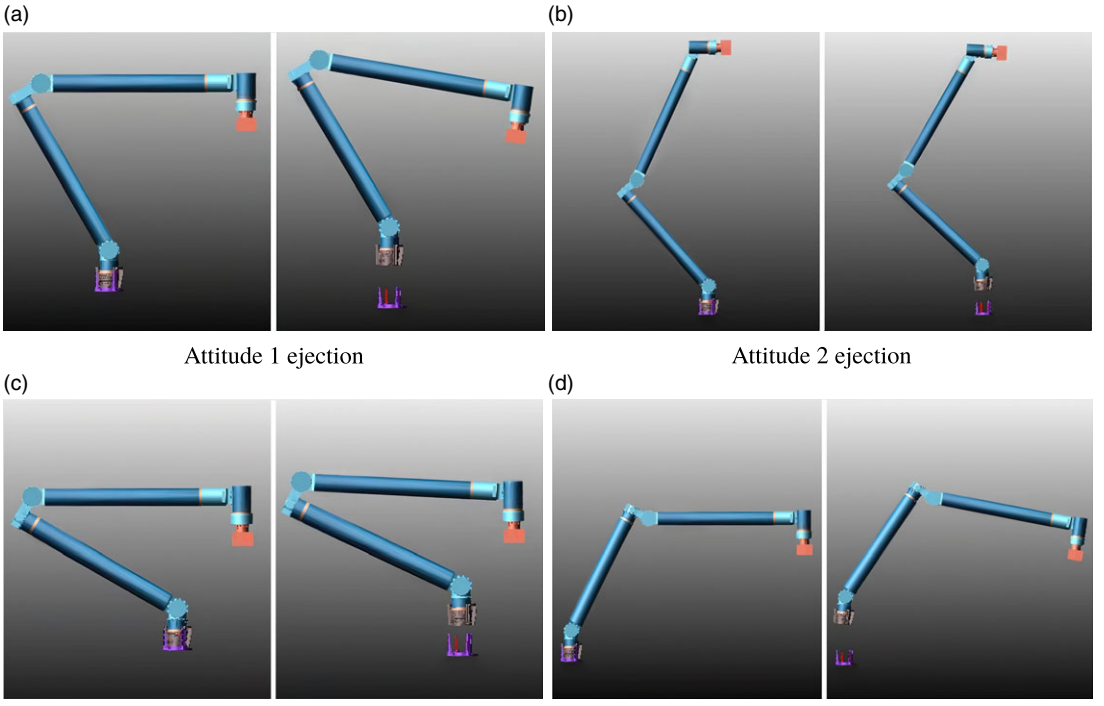


***Figure 7.*** *Simulation results of four attitudes of the manipulator.*

Table III presents the equivalent mass of the manipulator in the space state, plane state, and joint 4 free plane state under five attitudes. Air-floating support is included in the calculation of equivalent mass for all states except space, where no air-floating support exists. Meanwhile, the total mass of the manipulator and air-floating support is 116.1 kg. In space, the equivalent mass of attitude 3 is the smallest. In attitude 5, the manipulator is straight, and the joint rotation is minor, so the entire arm is equal to a single rigid body, and its equivalent mass is roughly equivalent to the overall mass of the manipulator. On the plane with the air-floating support, the equivalent mass of attitude 2 is the lowest. The theoretical calculation results of ejection time differ from the simulation results, with the largest difference of 2.6%. Further, the ejection velocity difference's largest value is 3.2%.

Figure 8 shows the ejection velocity of the movable base before the zero force separation. The ejection velocity trend of each attitude is consistent with the equivalent mass in the plane state shown in Table III. In the legend, "S" represents the simulation result and "T" represents the theoretical calculation result. The curves include the energy loss caused by the joint motion.

Figure 9 shows the angular velocity variance of the manipulator during ejection. Joints 2 and 4 still have relative rotation in each attitude after the manipulator's zero force separation. At this moment, the angular velocity of the movable base is the angular velocity caused by joint rotation, which is not the ejection angular velocity of the manipulator. In the process from zero force separation to stable ejection, the velocity of each arm of the manipulator changes from inconsistent to consistent, and the manipulator will generate rotating angular velocity. After the ejection is stable, the joints of the manipulator will not rotate, and the whole manipulator will eject at the same ejection velocity and angular velocity.

The ejection angular velocity of the manipulator remains unchanged when joints 2, 4, and 6 have no relative rotation, as can be determined from Eq. (42). When the manipulator is in attitude 4, its center of mass has the largest eccentricity and deviates to the right. The final ejection angular velocity is $-13.4°/s$, and the final ejection angular velocity of attitude 2 is $4.95°/s$.

https://doi.org/10.1017/S0263574723000747 Published online by Cambridge University Press

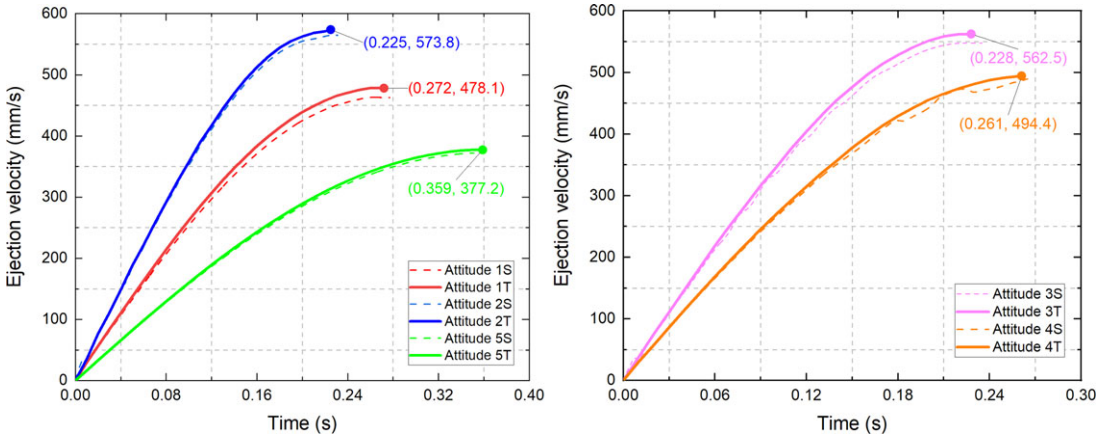


***Figure 8.*** *Simulation and theoretical results of ejection velocity.*

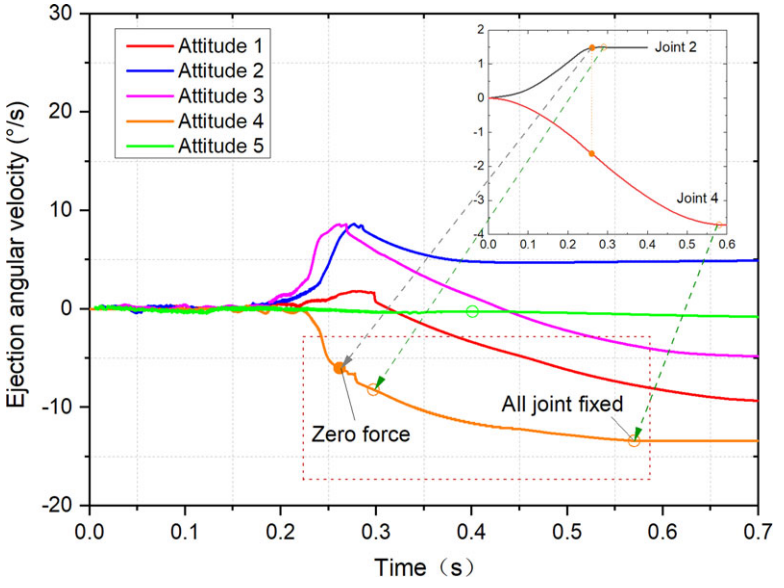


***Figure 9.*** *Simulation results of ejection angular velocity.*

Figure 10 shows the angular variation of joints 2 and 4 during ejection. It can be obtained by Eq. (29) when the manipulator is ejected inside ESD, and by Eq. (32) when the manipulator is ejected outside ESD. There is still relative rotation of the joint after the zero force separation.

## 5. Plane air-floating ejection test

### *5.1. Construction of plane air flotation test*

In the plane ejection test, as shown in Fig. 2, the ESD of the manipulator is fixed on the rigid bracket. The motion of the manipulator on the marble platform's plane is enabled by the air-floating support. An equivalent manipulator, which is consistent with the dynamic parameters of each part of the space manipulator, is used as the ejection test manipulator. The monitoring points are affixed on the movable base and each arm (Fig. 12). These monitoring points are observed by the high-speed camera to detect the ejection velocity of the movable base and joint angular variation at the time of zero force separation,

https://doi.org/10.1017/S0263574723000747 Published online by Cambridge University Press

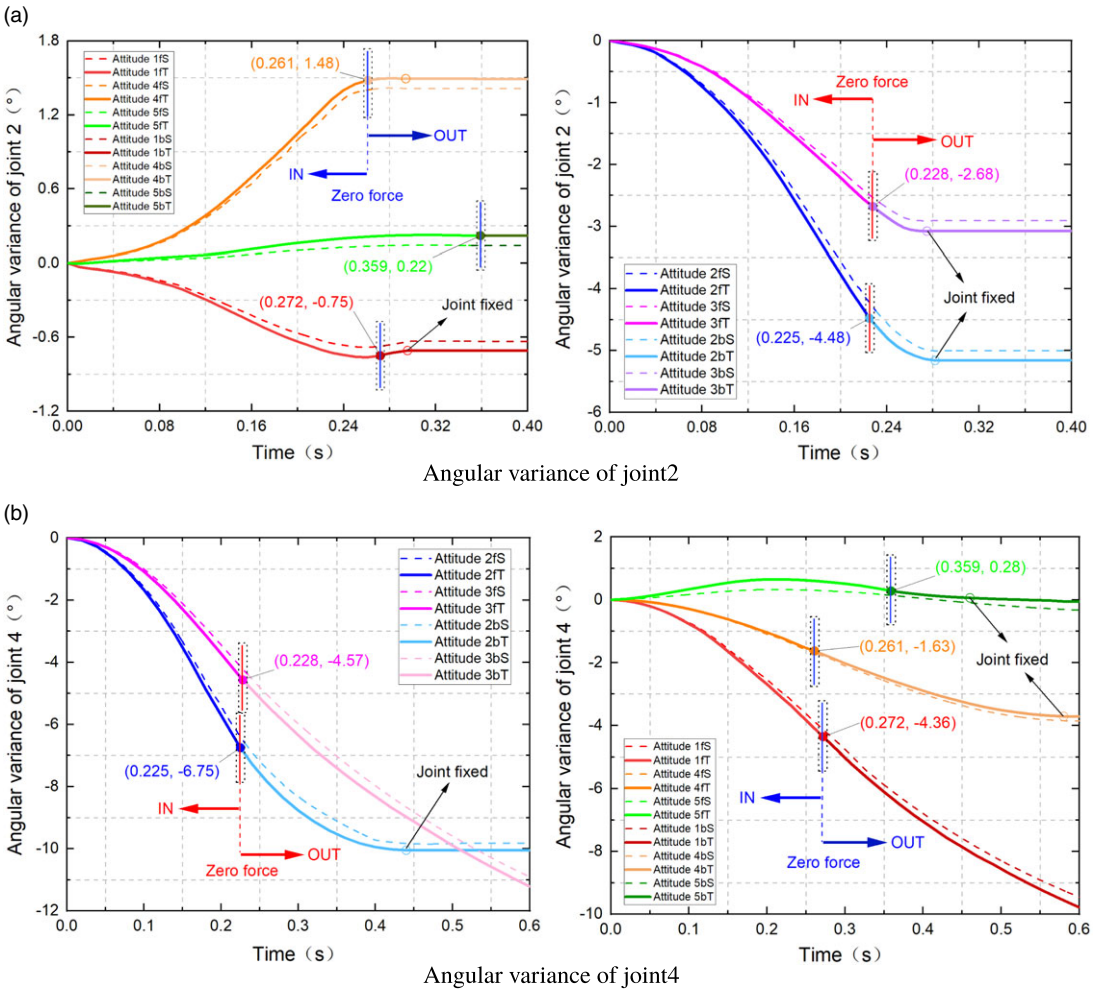


***Figure 10.*** *Simulation and theoretical results of angular variance of joints 2 and 4.*

respectively [25]. Then, the results of MATLAB theoretical calculation, ADAMS simulation, and plane air flotation test are compared.

### *5.2. Correction of joint damping B*

Figure 11 shows the ejection velocity curves of attitudes 3 and 4 under three different joint damping values. Since the joint angular variation of attitude 3 is larger than that of attitude 4, it is more sensitive to joint damping. The degree of bending of the attitude 3 curve increases with an increase in joint damping. When the joint damping increases 10 times, the bending degree of the ejection curve of attitude 3 is larger, while that of attitude 4 is smaller, and the final ejection velocity of attitude 4 is greater than that of attitude 3. Therefore, the joint dynamic friction torque and damping greatly influence on the ejection velocity of the joint with large variations.

As can be seen from Figs. 11 and 12, joint damping $B$ has an impact on the ejection velocity and the joint angular variation and has the greatest impact on attitudes 2 and 3, which has large joint angular variation. Therefore, the above two attitudes are considered as the basis for the correction of $B$.

https://doi.org/10.1017/S0263574723000747 Published online by Cambridge University Press

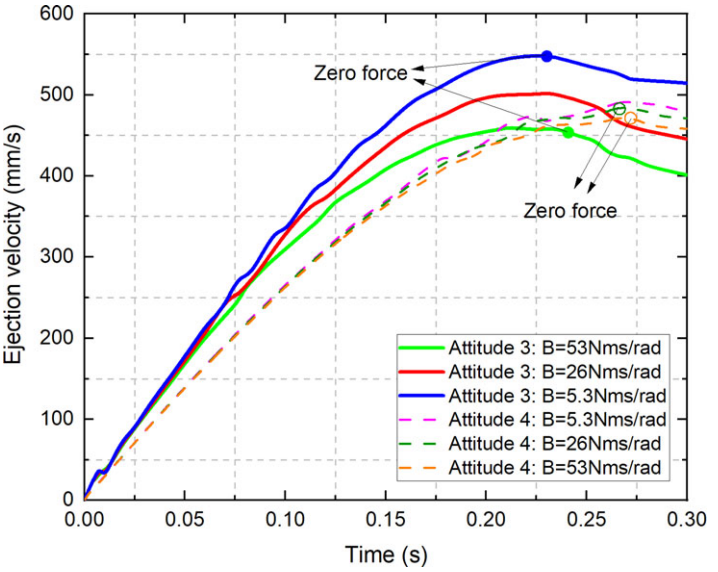


***Figure 11.*** *Simulation results with different joint damping.*

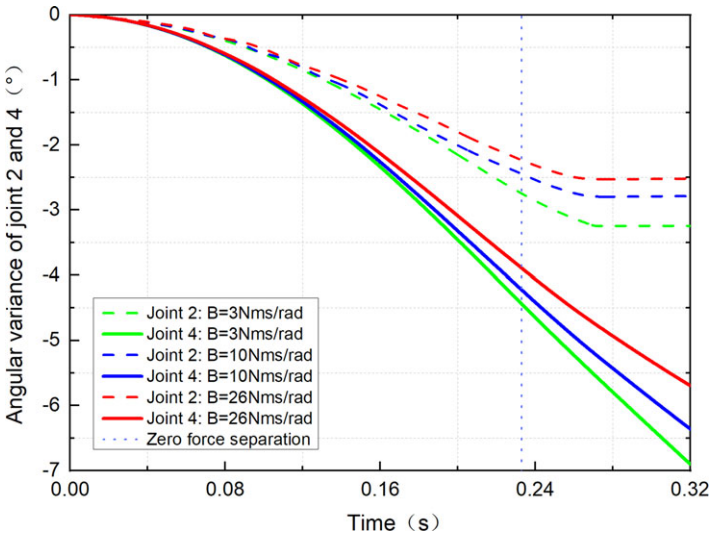


***Figure 12.*** *Joint angular variation of attitude 3 under different damping.*

Since the influence of joint angular variation has been considered in Eq. (36), the ejection velocity calculated by this equation contains information on joint angular variation. Thus, the ejection velocity error of calculation and test is taken as the correction target. Coefficient B was corrected by the least square method. Set the initial value $B_0 = 4.8$ Nms/rad (joint parameter identification) and incremental value $\Delta B = 0.2$ Nms/rad, then substitute damping $B_p = B_0 + p\Delta B$ into Eq. (43) and calculate $n$ times with the least square method:

$$J(B_p) = \sum_{j=2}^{3}\left[{}^{j}\bar{v}_{f0}(B_p) - \frac{1}{q}\sum_{i=1}^{q}{}^{j}v_t^i\right]^2, \quad p = 1, 2\cdots l \tag{43}$$

https://doi.org/10.1017/S0263574723000747 Published online by Cambridge University Press

***Table IV.*** *Dynamic parameters of manipulator with air-floating support.*

| | | Attitude | | | | |
|---|---|---|---|---|---|---|
| **Method** | | **1** | **2** | **3** | **4** | **5** |
| Ejection velocity | Theory | 478.1 | 573.8 | 562.5 | 494.4 | 377.2 |
| | Test | 446.8 | 540.6 | 534.3 | 456.2 | 364.2 |
| | error | 6.5% | 5.8% | 5.4% | 7.7% | 3.4% |
| Joint 2 angular variance | Theory | −0.75 | −4.48 | −2.68 | 1.48 | 0.22 |
| | Test | −0.92 | −4.99 | −3.24 | 1.80 | 0.31 |
| | error | 0.17 | 0.51 | 0.56 | 0.32 | 0.09 |
| Joint 4 angular variance | Theory | −4.36 | −6.75 | −4.57 | 1.63 | 0.28 |
| | Test | −3.81 | −7.53 | −4.09 | 1.92 | 0.31 |
| | error | 0.55 | 0.78 | 0.48 | 0.29 | 0.03 |

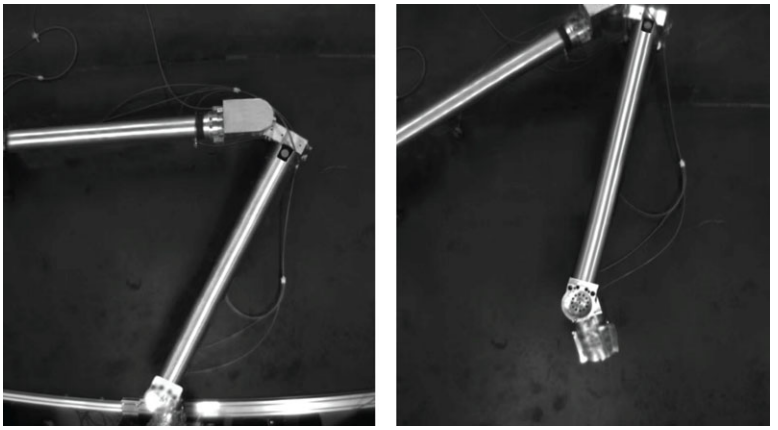

***Figure 13.*** *Attitude 1 ejection test.*

${}^{j}v_t^i$ is the ejection velocity of the movable base of the equivalent manipulator in the $i$th test (total $q$ times) under attitude $j$ at zero force separation time, and ${}^{j}\bar{v}_{f0}\left(B_p\right)$ is the ejection velocity calculated at joint damping $B_p$ under attitude $j$ at zero force separation time. After $l$ groups $J\left(B_p\right)$ are calculated, the joint damping $B$ corresponding to the minimum value $J(B_s)$ is taken as the revised $B_s$ value. The final value is $B_s = 5.4$ Nms/rad:

$$B_s = \min[J(B_1), J(B_2), \cdots J(B_l)] \tag{44}$$

Replacing the joint damping coefficient $B_s$ into the rest of the attitudes, the calculation and simulation results of the five attitudes are shown in Table IV. The maximum error between the test results and the calculated results of the ejection velocity is 7.7%, the maximum error between the test results and the calculated results of angular variance of joint 2 is 0.56°, and that of joint 4 is 0.78°. The primary source of error can be attributed to nonlinear factors such as the guiding stiffness, friction, and lubrication of the ESD, as well as the stiffness of the air-floating support and trachea. Among the tested attitudes, attitude 4 has the highest ejection velocity error, while attitude 5, in the straightening state with low nonlinear effects, has the lowest error.

Figure 13 shows the images taken by the high-speed camera before and after the ejection of the manipulator in attitude 1. There is an obvious angular variation of joint 4, and the manipulator has deflection caused by angular velocity.

https://doi.org/10.1017/S0263574723000747 Published online by Cambridge University Press

Then, the remaining attitudes were divided into the following two conditions for testing: the ejection tests are carried out when joint has friction torque and when the joint is completely locked. Through the above experiments, we have observed that the angles of joint 2 and 4 change obviously when there is friction torque, and there is a deflection caused by ejection angular velocity after ejection. After the manipulator is zero force separation, the angles of joints 2 and 4 still change. In order to maintain the consistency of multi-rigid body velocity, the ejection angular velocity also changes until the ejection angular velocity tends to be stable. However, when the joint was completely locked, the angle of the joint did not change, and the manipulator did not deflect obviously after ejection.

## 6. Conclusion

This study presents a space manipulator ejection dynamics model based on the kinetic energy equation, kinematics equation, and ejection boundary conditions. An equivalent mass calculation method for manipulator ejection and an approach to calculate the equivalent mass of the manipulator in the plane state by dimensional reduction are proposed. The study uses the ejection dynamics equation to obtain the ejection time, ejection velocity, and joint angular variation of the manipulator during ejection. The variation of equivalent mass and global inertial matrix during ejection are considered in calculating these ejection characteristics. The ejection angular velocity from zero force separation to stable ejection is then calculated according to the law of conservation of angular momentum.

Taking the manipulator with 7-DOF as an example, the ADAMS simulation and equivalent manipulator ejection test validated the correctness of the space manipulator ejection model. After revising the joint damping parameter B according to test results, the model has high accuracy, with merely a 3.2% error compared to the simulation results and an 7.7% error compared to the test results. Therefore, the model can be applied to the ejection calculation of other mechanisms with multi degree of freedom and non-fixed connection.

The study reveals that the kinetic friction torque and damping of joints play a significant role in determining the ejection velocity in certain attitudes. Furthermore, it analyzes the reasons for the generation of the ejection angular velocity of the manipulator in an ideal scenario involving slide rails.

**Author contributions.** All authors proposed the research and wrote the manuscript. Yanbo Wang instructed the research.

**Financial support.** This research received no specific grant from any funding agency, commercial, or not-for-profit sectors.

**Competing interests.** The authors declare no conflicts of interest exist.

**Ethical approval.** Not applicable.

## References

[1] W. M. Bao and X. W. Wang, "Prospect of airline-flight-mode aerospace transportation system," *Astronaut. Syst. Eng. Technol.* **5**(3), 1–6 (2021).
[2] W. L. Wang and J. Z. Yang, "Spacecraft docking & capture technology: Review," *Chin. J. Mech. Eng.* **57**(20), 215–231 (2015).
[3] C. Jiang and Z. K. Wang, "Angular velocity depressing method of constrained and centroid biased on-orbit separation," *Acta Aeronaut. Astronaut. Sin.* **36**(10), 3382–3392 (2015).
[4] C. Jiang, Z. K. Wang and Y. L. Zhang, "Study of on-orbit separation schemes for configuration initialization of fractionated spacecraft cluster flying," **In:** *Proceedings of the 1st IAA Conference on Dynamics and Control of Space Systems* (2012) pp. 1436–1448.
[5] A. K. Komarsofla, E. A. Yazdi and M. Eghtesad, "Dynamic modeling and control of a novel one-legged hopping robot," *Robotica* **39**(9), 1692–1710 (2021).
[6] P. Gallina, G. Bulian and G. Mosetti, "Water bouncing robots: A first step toward large-scale water running robots," *Robotica* **34**(7), 1659–1676 (2016).
[7] T. Senoo and M. Ishikawa, "Analysis of sliding behavior of a biped robot in centroid acceleration space," *Robotica* **35**(3), 636–653 (2017).

https://doi.org/10.1017/S0263574723000747 Published online by Cambridge University Press

[8] Z. G. Wang and Y. N. Yang, "Dynamics analysis of the spatial catapult separation problem," *Flight Dyn.* **32**(3), 239–252 (2014).
[9] H. Zhang and Y. Z. Xiao, "Study on on-orbit dynamic simulation of space docking mechanism separation," *J. Syst. Simul.* **26**(4), 954–958 (2014).
[10] J. Y. Zhang, *Non-liner Dynamic Research of Cubesats On-Orbit Deployment* (Harbin Institute of Technology, Harbin, 2017).
[11] C. Q. Luo, J. L. Sun and H. Wen, "Research on separation strategy and deployment dynamics of a space multi-rigid-body system," *Chin. J. Theor. Appl. Mech.* **52**(2), 503–513 (2020).
[12] G. Chen, D. Liu and Y. Wang, "Contact force minimization for space flexible manipulators based on effective mass," *J. Guid. Control Dyn.* **42**(8), 1870–1877 (2019).
[13] M. Ahmadizadeh, A. M. Shafei and M. Fooladi, "Dynamic analysis of multiple inclined and frictional impact-contacts in multi-branch robotic systems," *Appl. Math. Modell.* **91**, 24–42 (2021).
[14] W. Yan, Y. Liu and Q. Lan, "Trajectory planning and low-chattering fixed-time nonsingular terminal sliding mode control for a dual-arm free-floating space robot," *Robotica* **40**(3), 625–645 (2022).
[15] K. Yoshida and N. Sashida, "Modeling of impact dynamics and impulse minimization for space robots," **In:** *IEEE/RSJ Intemational Conference on Intelligent Robots and Systems* (IEEE, 1993) pp. 2064–2069.
[16] H. L. Zhang and X. Liao, "Research on performance validation of aircraft based on air-table," *J. Syst. Simul.* **30**(10), 3739–3745 (2018).
[17] J. K. Jae and N. A. Brij, "Automatic mass balancing of air-braing-baesd three-axis rotational spacecraft simulator," *J. Guid. Control Dyn.* **32**(3), 1005–1017 (2009).
[18] M. H. Korayem and S. F. Dehkordi, "Dynamic modeling of flexible cooperative mobile manipulator with revolute-prismatic joints for the purpose of moving common object with closed kinematic chain using the recursive Gibbs-Appell formulation," *Mech. Mach. Theory* **137**, 254–279 (2019).
[19] M. H. Korayem and A. M. Shafei, "Motion equation of nonholonomic wheeled mobile robotic manipulator with revolute-prismatic joints using recursive Gibbs-Appell formulation," *Appl. Math. Modell.* **39**(5-6), 1701–1716 (2015).
[20] V. Mata, S. Provenzano and F. Valero, "Serial-robot dynamics algorithms for moderately large numbers of joints," *Mech. Mach. Theory* **37**(8), 739–755 (2002).
[21] M. H. Korayem and S. F. Dehkordi, "Derivation of motion equation for mobile manipulator with viscoelastic links and revolute-prismatic flexible joints via recursive Gibbs-Appell formulations," *Rob. Auton. Syst.* **103**, 175–198 (2018).
[22] Y. Zhu and S. L. Wang, "Analytical solution for vibration system with time-varying mass," *J. Vibr. Shock* **27**(11), 160–167 (2008).
[23] D. N. Nenchev and K. Yoshida, "Impact analysis and post-impact motion control issues of a free-floating space robot subject to a force impulse," **In:** *IEEE Intemational Conference on Robotics and Automation* (IEEE, 1999) pp. 548–557.
[24] G. Chen, Q. X. Jia and H. X. Sun, "Analysis on impact motion of space robot in the object capturing process," *Robot* **32**(3), 432–438 (2010).
[25] O. Ma, H. Dang and K. Pham, "On-orbit identification of inertia properties of spacecraft using a robotic arm," *J. Guid. Control Dyn.* **31**(6), 1761–1771 (2012).

**Cite this article:** H. Cai, Y. Wang, S. Deng and T. Yang (2023). "Emergency ejection characteristics of space manipulator multi-body system", Robotica **41**, 3252–3274. https://doi.org/10.1017/S0263574723000747